AER

ATMOSPHERIC & ENVIRONMENTAL RESEARCH, INC.
Cambridge, Massachusetts

OUTER SATELLITE ATMOSPHERES: THEIR NATURE AND PLANETARY INTERACTIONS

Annual Report for Period
June 1, 1981 to May 31, 1982

Prepared for
NASA Headquarters
Washington, DC 20546

Prepared by
William H. Smyth
Atmospheric and Environmental Research, Inc.
840 Memorial Drive
Cambridge, Massachusetts 02139

TECHNICAL REPORT STANDARD TITLE PAGE

1. Report No.	2. Government Accession No.	3. Recipient's Catalog No.

4. Title and Subtitle	5. Report Date
Outer Satellite Atmospheres: Their Nature and Planetary Interactions	July 1982
	6. Performing Organization Code
7. Author(s) William H. Smyth	8. Performing Organization Report No.
9. Performing Organization Name and Address Atmospheric and Environmental Research, Inc. 840 Memorial Drive Cambridge, Massachusetts 02139	10. Work Unit No.
	11. Contract or Grant No. NASW-3387
	13. Type of Report and Period Covered Annual Report June 1, 1981 - May 31, 1982
12. Sponsoring Agency Name and Address NASA Headquarters Headquarters Contract Division Washington, DC 20546	14. Sponsoring Agency Code HW-2

15. Supplementary Notes

16. Abstract

The Io sodium cloud model has been successfully generated to include the time and spatial dependent lifetime sink produced by electron impact ionization as the plasma torus oscillates about the satellite plane, while simultaneously including the additional time dependence introduced by the action of solar radiation pressure on the cloud. Very preliminary model results are discussed and continuing progress in analysis of the peculiar directional features of the sodium cloud is also reported. Significant progress has been made in developing a model for the Io potassium cloud and differences anticipated between the potassium and sodium cloud are described. An effort to understand the hydrogen atmosphere associated with Saturn's rings has been initiated and preliminary results to date of a survey and study are summarized.

17. Key Words (Selected by Author(s))	18. Distribution Statement
satellite atmospheres planetary magnetospheres comets	

19. Security Classif. (of this report)	20. Security Classif. (of this page)	21. No. of Pages	22. Price*
Unclassified	Unclassified	119	

*For sale by the Clearinghouse for Federal Scientific and Technical Information, Springfield, Virginia 22151.

TABLE OF CONTENTS

LIST OF FIGURES

LIST OF TABLES

I. INTRODUCTION

The research program is organized into three different subjects: (1) the Jupiter system, (2) the Saturn system, and (3) comets. In the Jupiter system, the extended atmospheres of Io and their relations and interactions with the planetary magnetosphere are the topics of interest. In the Saturn system, the hydrogen torus of Titan, the atmospheres associated with the planetary rings, and the extended atmospheres of the E-Ring satellites are the topics of concern. For comets, the dust and gas clouds in the outer coma are the area of focus.

Research efforts for the extended atmospheres of Io are divided into the study of the Io sodium cloud, the Io potassium cloud, and other gas clouds of Io. The effort discussed here represents a logical continuation, extension and expansion of our prior programs supported by NASA. A condensed summary of our prior and present programs is given in Table 1. As is shown in Table 1, the study of the Io sodium cloud is further divided into four separate topics organized around different types of observational data that are available. Efforts in the first year of this program have been primarily focused upon model improvement or development for the topics 1(i), 1(iii) and 2 in Table 1, and upon exploratory investigation for the topic 1(iv). The topic 1(ii) has remained inactive, waiting for the first year improvements in the model to be completed and the topic 3(ii) will be activated when relevant new information becomes available.

The research effort for the Saturn system also represents a logical continuation and an extension of our prior programs supported by NASA. A brief summary of the content of the prior and present programs is given in Table 2. As can be seen in Table 2, the Titan hydrogen torus has been a long-standing topic, whereas interest in the extended ring and E-ring satellite atmospheres has been initiated more recently as a result of the Pioneer 11, Voyager 1 and Voyager 2 encounters with Saturn. For this reason, effort in the first year of the program has placed primary emphasis upon topic 2, where some data are now available, and minor effort on topics 1 and 3. These latter two topics will receive increased emphasis in the work to be performed in the second and

Table 1

Research Program: Extended Atmospheres of Io

		Past AER Effort			Proposed AER Effort
1.	Io Sodium Cloud	1978	1979	1980	1981-1984
	(i) 2-D Intensity Distribtuion	Model analysis of 56 2-D images (Smyth & McElroy, 1978)	Discovered solar radiation pressure mechanism (Smyth, 1979)	Constructed 3-D model for solar radiation pressure effects	Investigate effects of the Io plasma torus on 2-D distribution with solar radiation pressure effects
	(ii) Line Profile Studies	-	Studied effects of solar radiation pressure and satellite phase angle	Studied correlation of spectral and spatial effects of high-speed sodium emission from Io	Perform model calculation and compare with new data
	(iii) Interaction with the Io Plasma Torus	-	Preliminary model calculations for neutral cloud and ion source	2-D plasma torus description developed for sodium cloud model	Improve torus description in sodium cloud model and evaluate its effect
	(iv) Peculiar Linear Features	-	-	Developed model to describe local enhanced ejection of sodium	Refinement of model and comparison with data
2.	Io Potassium Cloud	-	-	-	Develop and compare model results with new data
3.	Other Gas Clouds of Io				
	(i) 2-D Intensity Distribtuion of Oxygen and Sulfur; Satellite Ion Source	-	-	Constructed 3-D model for oxygen cloud and its ion source	Continuation under JDAP support
	(ii) Exploratory Modeling of new Clouds	-		-	Model development and application

TABLE 2

RESEARCH PROGRAM: SATURN SYSTEM AND COMETS

	Past AER Effort			Proposed AER Effort
	1978	1979	1980	1981-1984
Extended Atmospheres of the Saturn System				
1. Titan Hydrogen Torus	Model Development	Pre-Pioneer Encounter Model Calculation for Cloud and Ion Source	Post-Pioneer Encounter Model Calculation for Cloud and Ion Source (Smyth, 1981)	Comparison of Model with Voyager Data
2. Saturn Rings	--	--	Model under Development	Comparison of Model with Pioneer and Voyager Data
3. E-Ring Satellite	--	--	Exploratory Calculation Performed	Consider Exploratory Calculation where Warranted by Voyager Data
Extended Atmospheres of Comets	--	--	Model under Development	Incorporation of Model Refinements and Application to Observations

third years (see Appendix A for a brief post-Voyager update on the Titan hydrogen torus).

For comets, the research program here represents a continuing of effort to refine our basic exospheric model for comets used for interpretive analysis of both dust and neutral gaseious components in the coma. The prior and present programs for this development are also summarized in Table 2. No effort to continue this development was scheduled during this first program year in order that more emphasis could be placed upon the model developments and improvements scheduled under topics 1(i) and 1(iii) of Table 1. The necessary refinements and the subsequent application of the comet model are to be suitably scheduled during the next two years.

In Sections II, III and IV, the progress and significant accomplishments of the first year of the program are summarized. References are given in Section V and Section VI, and are followed in Section VII by the Appendices containing supporting information.

II. PROGRESS IN MODELING THE IO SODIUM CLOUD

2.1 Model Development

The primary focus of our effort during the first year for the Io sodium cloud has been the generalization of the cloud model to include the time and spatial dependent sink produced by the oscillation of the Io plasma torus about the satellite plane. Electron impact ionization of sodium atoms by torus electrons provides the only sink mechanism considered to date, but elastic collision of sodium cloud atoms and plasma torus ions may also possibly contribute (Brown, Pilcher and Strobel, 1981). The importance of the elastic collisions will be evaluated in the second year effort.

The oscillation of the plasma torus about the satellite plane introduces several different and distinct time dependences into the sodium cloud for an earth observer. Relative to the satellite, the period of oscillation of the plasma torus is about 13 hours and this will produce a time dependent sink for the cloud with observed intensity changes on the order of a few hours. Such changes have been observed and attributed by Trafton (1977, 1980) to the oscillating torus. Apparent time dependent changes in the two-dimensional morphology of the cloud also occur on a longer time scale for an earth observer because of the periodic motion of Io about its circular orbit (~42.5 hour) and the different geometrical projections of the cloud intensity on the sky plane. Because of the non-synchronous values of the oscillatory and orbital periods, the sodium cloud on the sky plane will actually appear to have a longer effective period of about 25 Io rotations or 44.25 days. Real time dependent changes having this same 44.25 day period will also be introduced because of the east-west cloud distribution asymmetry which is driven by solar radiation pressure (Smyth, 1979, 1982). These real time changes occur because the envelope of the sodium cloud changes shape as a function of the satellite phase angle and therefore has a different spatial overlap with the oscillating plasma torus for each different angular location of the satellite on its orbit about Jupiter. This different spatial overlap is illustrated for two diametrically opposite satellite phase angles in Figure 1 and is described in more detail in Appendix B.

Figure 1. Interaction of the Sodium Cloud and the Plasma Torus. The spatially-projected overlap in the satellite plane of the Io plasma torus with the solar radiation perturbed cloud shape (solid boundary with heavy shading) and with the unperturbed cloud shape (heavy dashed boundary) is indicated for the diametrically opposite satellite phase angles.

The generalization of the sodium cloud model to include the oscillating plasma torus requires processing the time history of many atom orbits as they travel through the oscillating torus. This time processing, although relatively straight forward, involves careful alteration and considerable expansion of the previous existing computational code with special emphasis placed upon execution efficiency. Steady and substantial progress has been made and the first phase, that of model development to include the oscillating torus excluding the effects of solar radiation pressure, has been successfully completed. The second phase, that of adding the effects of solar radiation pressure to the generalized code structure created in the first phase, was just completed at the end of this first program year. The improved model is capable of calculating the two-dimensional density and intensity distributions of the sodium cloud on the sky plane [topic 1(i) of Table 1] as well as the shape of the spectral line profile seen through a prescribed viewing aperture [topic 1(ii) of Table 1]. The model is also capable of calculating the instantaneous and thirteen-hour cumulative spatial distribution of sodium ions deposited in the planetary magnetosphere.

Very preliminary results for the model developed under phase one have been obtained during code refinements and code testing. A "one-orbit-run" option was mostly used in these tests instead of the full set of orbits necessary to provide the complete spatial statistics for the cloud. This allowed the code to be thoroughly tested while at the same time minimizing the CPU computing expenses incurred. Fluctuations by a factor of two or more in the cloud density north and south of Io were obvious in these test runs and were correlated with the spatial location of the oscillating torus. The average lifetime of sodium in the cloud increased significantly because of the oscillating torus and provided an increased abundance of sodium in the cloud for a given escape flux at Io when compared to the non-oscillating computation. Sodium ions that were created were preferentially deposited near the intersection of the satellite orbit plane and the centrifugal plane of the plasma torus. In the beginning of the second program year, preliminary results will be calculated for the full model completed under phase two of the development.

2.2 Io Plasma Torus

Efforts to improve the description of the Io plasma torus in the Io sodium cloud model have been undertaken simultaneously with the model development summarized in the previous sub-section. The lifetime of sodium atoms in the plasma torus due to electron impact ionization is presented in Figure 2. The calculation is based upon the best available information from analysis of Voyager 1 data. Electron densities derived from plasma data by Bagenal and Sullivan (1981) and electron temperatures deduced both from UVS data by Shemansky (1980) and from in situ plasma measurements by Scudder, Sittler and Bridge (1981) were used.

In Figure 2, the lifetime of sodium atoms is seen to be as small as about one hour near Io and to increase at Io's location during the 7 degree oscillation of the plasma torus about the satellite plane to a value of about 4 hours. Along the centrifugal equator, the lifetime of sodium is extremely asymmetric about Io's orbital location. This asymmetric character will allow atoms which travel inside of Io's orbit to have a larger survival lifetime than atoms that travel outside of Io's orbit. This difference in survival lifetime may provide a basis for explaning the previously assumed asymmetric inner-hemisphere source of sodium used to match observational data in model calculations where the plasma torus was not included. Future model calculations to be performed in the second year will explore this possibility more fully.

Efforts to extend the accuracy of the plasma torus description in the model, especially for radial distances larger than 8 Jupiter radii, have also been pursued during the first year. Voyager 1 in situ plasma data describing the complete radial region from 4.9 to 21 Jupiter radii have been obtained from Belcher (1981) and are under study for this reason. A suitable description for the plasma density in this extended radial region has been adapted from this study and will be incorporated in the model in the second program year. Ground-based observations (Pilcher et al., 1981; Trauger, 1981) showing changes in the plasma properties with the λ_{III} magnetic coordinate will be incorporated in the future when a definite functional dependence can be established.

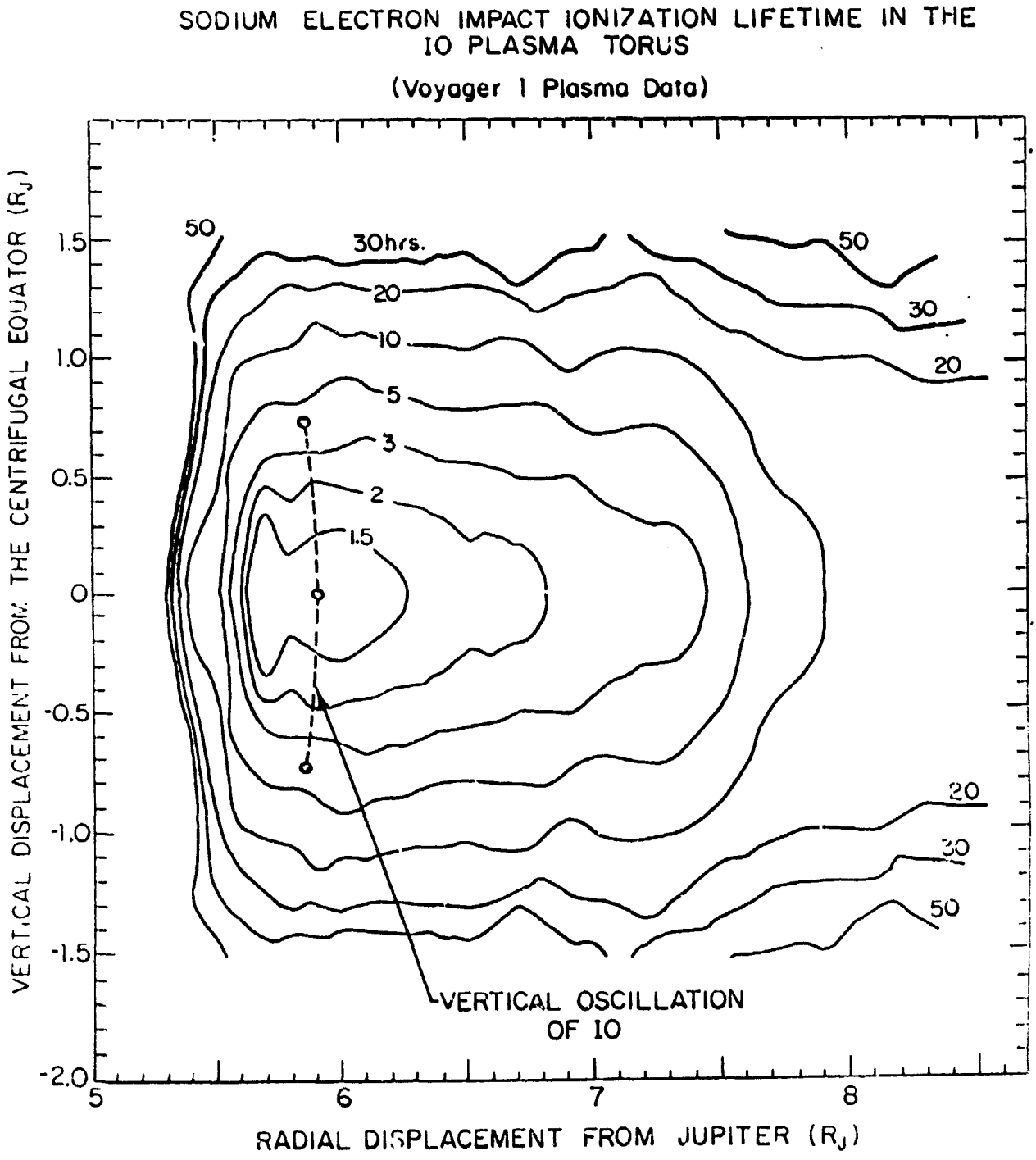

Figure 2. Sodium Electron Impact Ionization in the Io Plasma Torus. The lifetime calculation is based upon the plasma data referenced in the text. The two-dimensional common temperature model of Bagenal and Sullivan (1981) was selected to describe the electron density.

2.3 Directional Features

The peculiar directional features, discovered by Pilcher (1980) and also observed by Goldberg (1981), represent one of the newest phenomena of the sodium cloud to be documented. From the data of Pilcher (1981), these directional features are seen to be somewhat transient in nature and are usually observed outside of Io's orbit as faint extensions to the bright sodium cloud. These features many times appear to be inclined about 20 degrees with respect to the satellite plane and sometimes appear above and sometimes appear below the satellite plane.

Preliminary modeling analysis of Pilcher's data for these 20 degree inclined features, undertaken in the first year, suggests that high speed sodium (6-10 km/sec) is emitted near Io with a velocity vector most likely in the forward direction of motion of the satellite and has a similar inclination angle with respect to the satellite orbit plane. Analysis of more data will be required to determine if this high-speed emission is localized on the satellite surface, or if the emission results from the magnetospheric wind that moves past Io. In the latter case, such a high-speed stream of sodium might be driven by elastic collisions of sodium atoms with plasma torus ions (Brown, Pilcher and Strobel, 1981) and provide a source for the remote sodium cloud observed outside of the Io orbit by Brown and Schneider (1981).

The possible magnetospheric wind emission process is illustrated in Figure 3 and contrasted with an inner hemisphere emission process. The inner hemisphere emission process was required for much lower velocities ($\sim$2.6 km sec^{-1}) in earlier models of Smyth and McElroy (1978), which predated the discovery of the Io plasma torus, to obtain reasonable agreement withthe two-dimensional morphology of the bright sodium cloud observed by Murcray and Goody (1978). The actual initial velocity distribution at Io is likely broad (0-18 km sec^{-1}) with a peak value probably at the lower emission velocities. One method being studied to help determine the actual relative weights in the initial velocity distribution is that of using the sodium model including the ionization effects of the plasma torus to study data (Pilcher, 1981) for the time evolution of the directional features. Such a study may also be important in evaluating if there is a variable flux of sodium escaping from Io's exosphere which is modulated through the magnetospheric wind interaction by the oscillatory motion of the plasma torus about the satellite.

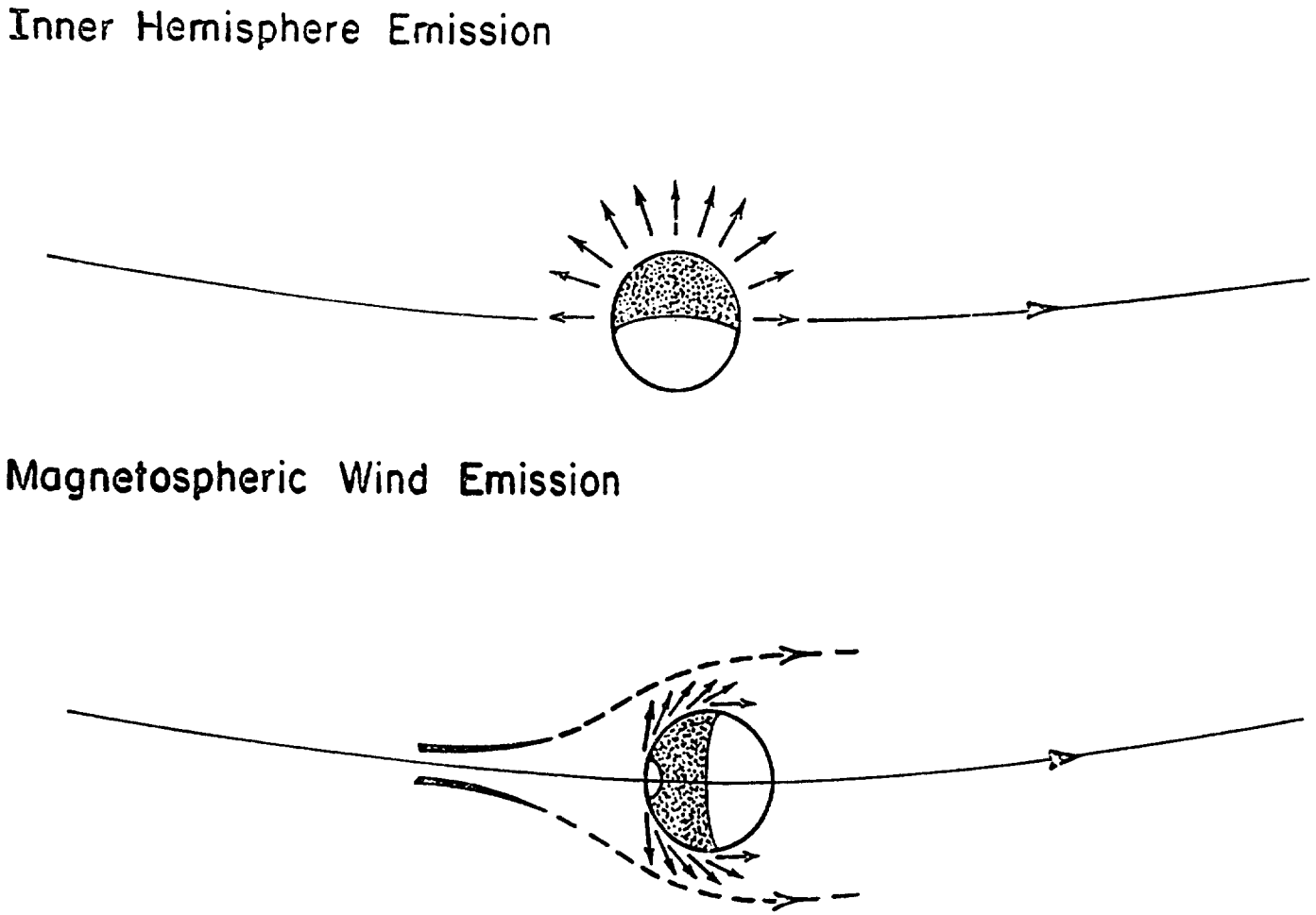

Figure 3. Emission of Sodium from Io. Two rather different schemes by which sodium may be emitted from Io are illustrated.

III. PROGRESS IN MODELING THE IO POTASSIUM CLOUD

3.1 Introduction

The Io potassium cloud has been observed to radiate in the 7665 Å and 7699 Å lines by Trafton (1975a). The radiation is thought to arise from solar resonance scattering. Observations of Trafton (1977, 1981a) have shown that the Io potassium cloud exhibits spatial and temporal variations similar to those observed for the sodium cloud. These observations indicate that the potassium cloud undergoes periodic fluctuations in response to solar radiation pressure (producing the east-west asymmetries) and in response to the ionizing influence of Jupiter's plasma torus (producing the north-south asymmetries). In addition, temporary directional features of potassium from Io have also been observed. Modeling improvements for the sodium cloud model discussed in the preceeding subsection may therefore be applied directly to our future development of an Io potassium cloud model.

Efforts in the first program year have been scheduled to obtain the necessary information for potassium required for converting, in the second program year, the Io sodium cloud model to the Io potassium cloud model. This information consists of the electron impact ionization lifetime of potassium in the Io plasma torus, the solar spectrum for each potassium line, and the acceleration experienced by potassium atoms as they undergo solar resonance scattering. All this information has been acquired in the first program year and is summarized below.

3.2 Io Plasma Torus

The electron impact ionization lifetime of potassium in the Io plasma torus has been calculated and is presented in Figure 4. The calculation is based upon the same Voyager 1 data used in determining the sodium lifetime in Figure 3. On the centrifugal equator, the potassium lifetime is slightly smaller near Io's orbital location and has a less steep gradient with increasing radial displacement from Jupiter than does the sodium lifetime. The ionizing impact of the plasma torus on the potassium cloud may, therefore, be expected to be slightly more severe than for the sodium cloud in our future modeling.

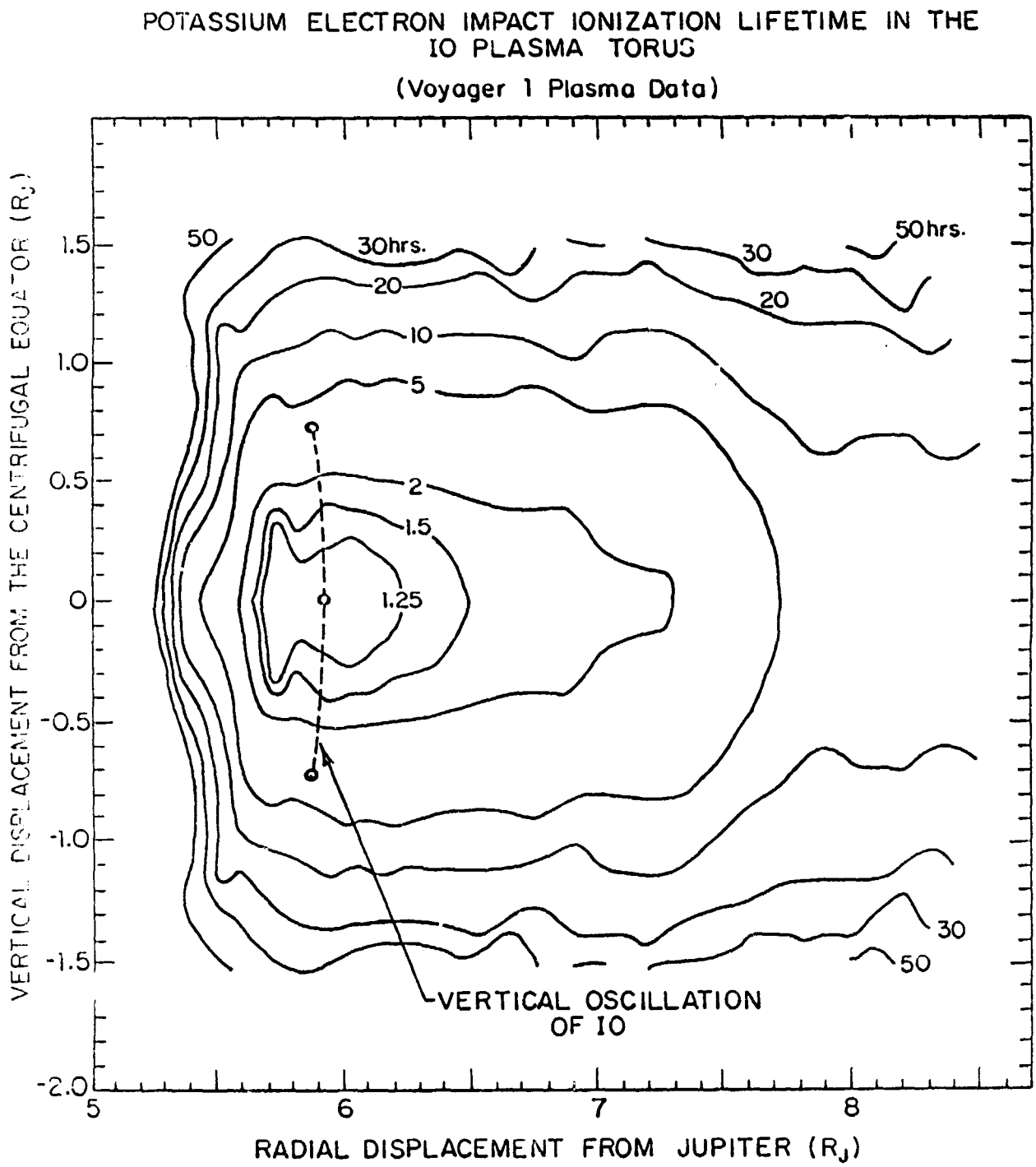

Figure 4. Potassium Electron Impact Ionization in the Io Plasma Torus. See legend to Figure 2.

3.3 Solar Spectrum for the Potassium Lines

Both of the potassium lines appear in solar absorption features, and the line at 7665 Å is almost completely obscured to a ground-based observer because of an optically thick oxygen absorption feature present in the earth's atmosphere. To properly model the intensity morphology of the cloud or the line profile shape in the 7665 Å emission, the exact shape of the solar absorption feature above the earth's atmosphere must be known. The computation of the unobstructed solar absorption feature and the earth's atmospheric transmission function has been provided in this program year by Kurucz (1982) with whom a collaborative effort for this purpose has been established. The results of his computation are presented and discussed below.

The calculated solar spectrum above the earth's atmosphere, the calculated transmission function of the earth's atmosphere at the Kitt Peak Observatory and the calculated and measured solar spectra at the location of the Kitt Peak Observatory are given in Figure 5 and Figure 6 for the potassium lines at 7699 Å and 7665 Å respectively. The calculated and measured spectra are in excellent agreement and differ at most by 1%. For the potassium line at 7699 Å in Figure 5, the atmospheric transmission is essentially 100% except for the two very small absorption features in its far wings. The depth of the potassium feature at 7699 Å is about 19% of the continuum value at line center and the wings of the feature above the earth's atmosphere are essentially symmetric. For the potassium line at 7665 Å in Figure 6, the earth's atmospheric transmission function is zero or small over much of the solar absorption feature. Above the earth's atmosphere, the potassium feature has a depth of about 14% at line center and the wings of the feature are asymmetric about the line center. This asymmetry results because of weak CN solar absorption features at 7664.316 Å, 7664.404 Å, 7664.533 Å and 7664.550 Å and stronger Fe solar absorption features at 7664.162 Å, 7664.305 Å and 7664.411 Å.

The physical implications of the solar spectra and the earth's atmospheric transmission functions presented above may be translated into interesting effects in the observed and modeled spatial and spectral characteristics of the Io potassium cloud. Two different types of effects should be distinguished. First, there are brightness varia-

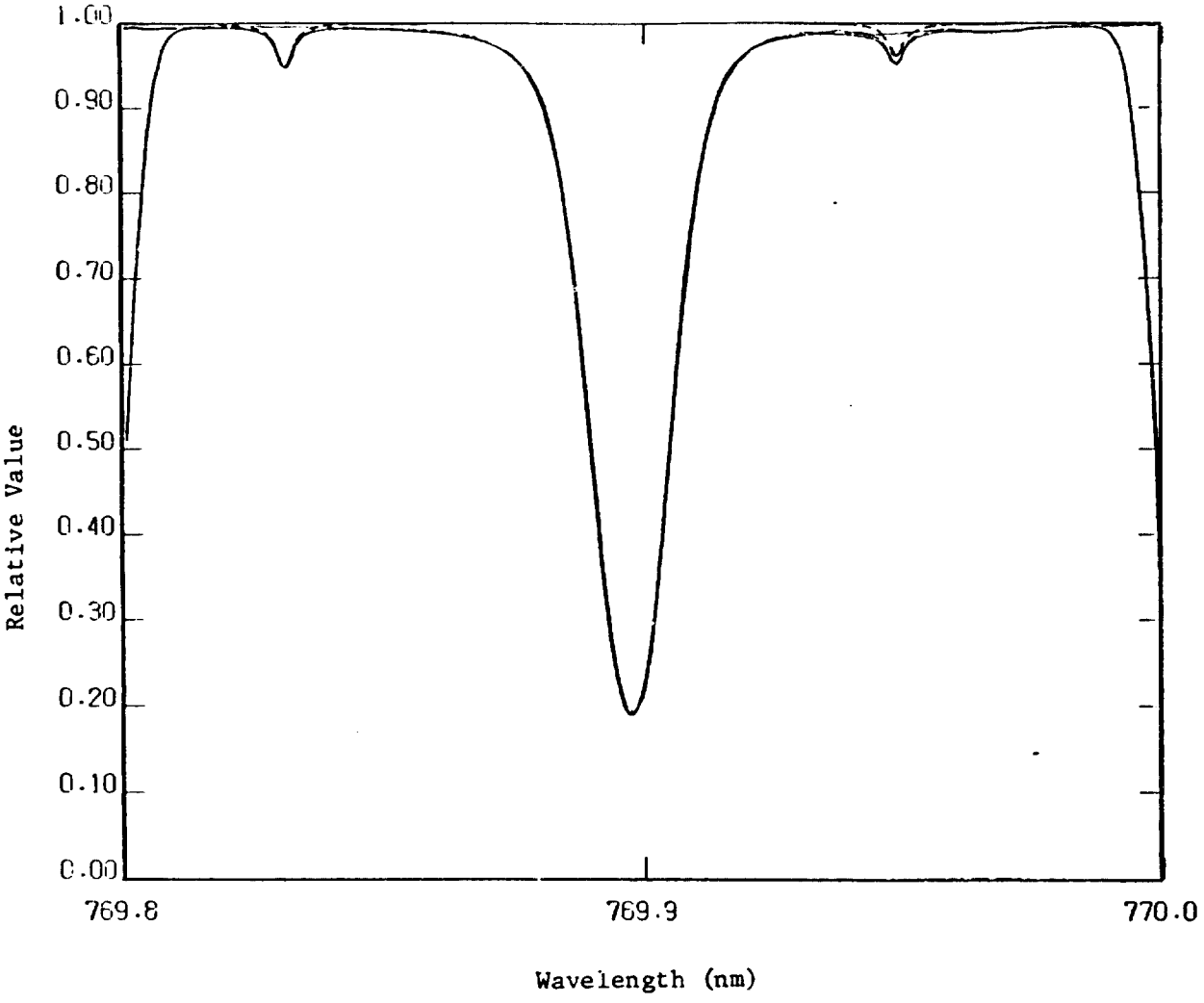

Figure 5. Solar Spectra and Earth's Atmospheric Transmission Function for the 7699 Å Potassium Line. The solar spectrum above the earth's atmosphere, indicated by the light-weight line, and the earth's atmospheric transmission function for the location of the Kitt Peak Observatory, indicated by the dashed line, were both calculated by Kurucz (1982). The solar spectrum observed at the location of the Kitt Peak Observatory is indicated by the heavy-weight line and the predicted shape of this spectrum (Kurucz, 1982) in the plot is indistinguishable. The downard trend of the spectrum on the left and right boundaries of the plot is instrumental in origin.

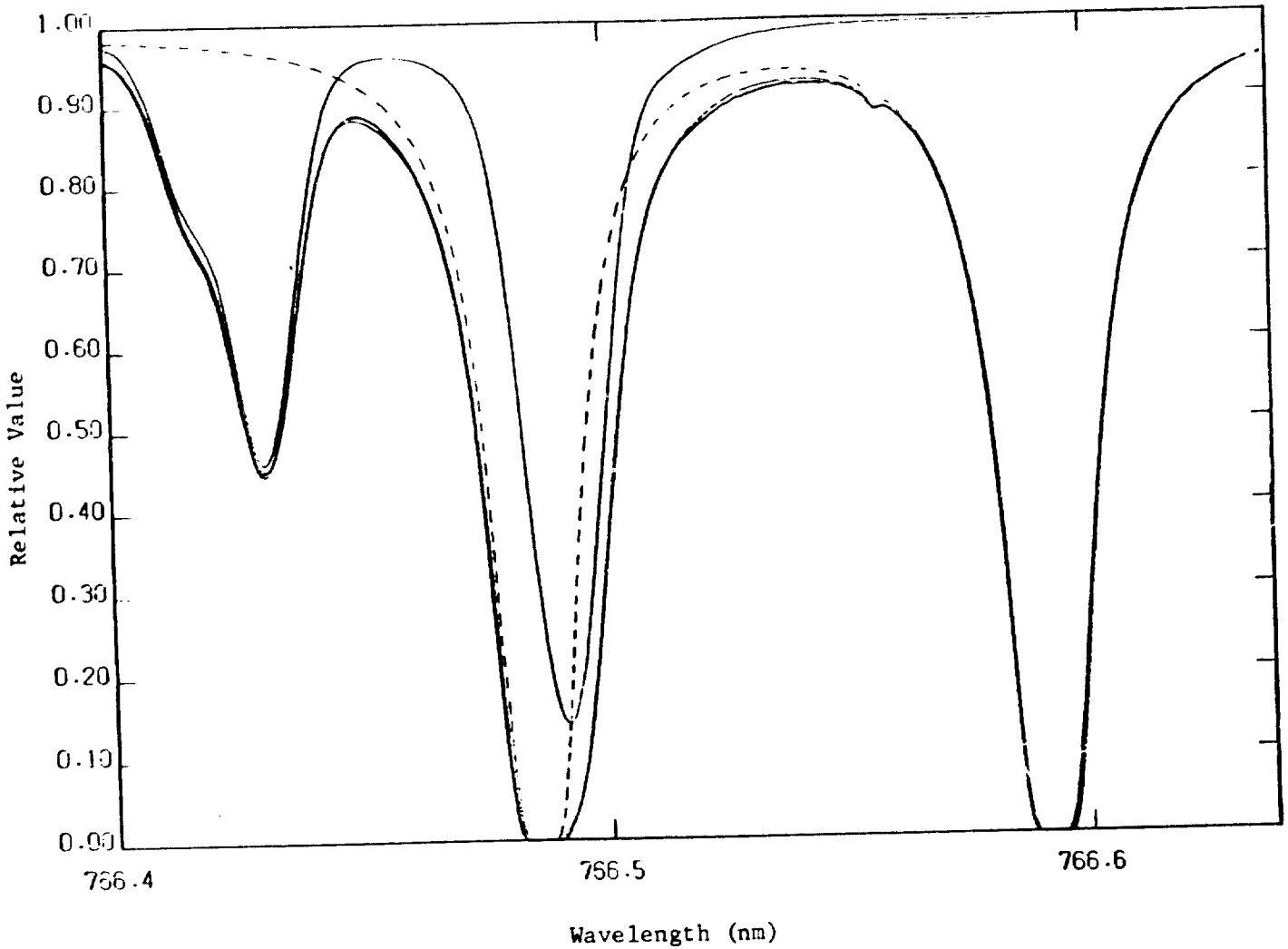

Figure 6. Solar Spectra and Earth's Atmospheric Transmission Function for the 7665 Å Potassium Line. The solar spectrum above the earth's atmosphere, indicated by the light-weight line (not the one plotted very near the heavy-weight line), and the earth's atmospheric transmission function for the location of the Kitt Peak Observatory, indicated by the dashed line, were both calculated by Kurucz (1982). The solar spectrum observed at the location of the Kitt Peak Observatory is indicated by the heavy-weight line and the predicted shape of this spectrum (Kurucz, 1982) by the light-weight line that is plotted very near the heavy-weight line.

tions introduced because the intensity contribution available for solar resonance scattering by a potassium cloud atom depends upon the shape of the solar spectrum and the amount of Doppler shift along this spectrum produced by the relative radial motion between the atom and the sun. Second, there will be additional brightness impediments for a ground-based observer which are introduced by the shape of the earth's atmospheric transmission feature and the amount of Doppler shift along this transmission spectrum produced by the Earth-Jupiter velocity and the motion of the cloud about Jupiter. These two effects are discussed below.

The radial velocity between a potassium cloud atom and the sun varies from nearly zero to a value as large as 20 km sec^{-1} to 35 km sec^{-1} and will provide a Doppler shift from line center as large as 500 ma to 875 ma. Doppler shifts of only about 250 ma are required for the potassium atom wavelength to be shifted from its line center to its wing. Larger Doppler shifts can only provide a significant change in the intensity of the 7665 Å spectrum, and then only for Doppler shifts larger than 400 ma to shorter wavelengths (when the potassium cloud is observed near western elongation) because of the presence of the strong Fe absorption feature in the solar spectrum (see Figure 6). The radial velocity between the potassium cloud and the earth may vary from nearly zero to a value as large as 40 km sec^{-1} to 65 km sec^{-1} and will provide Doppler shifts as large as 1.0 Å to 1.625 Å relative to the wavelength scale of the earth's atmospheric transmission function. For the 7665 Å line, Doppler shifts between 0.75 Å and 1.25 Å to a larger wavelength will be located in the next adjacent oxygen absorption feature (see Figure 6) so that care must be taken in comparison of observed and calculated spatial intensities or high-resolution line profile shapes to properly account for the atmospheric transmission function.

3.4 Solar Resonance Scattering

From Figure 5 and Figure 6, the potassium lines at 7699 Å and 7665 Å are seen to be located in solar absorption features with depths, respectively, of about 19% and 14% of the continuum level and with widths of about ±250 mÅ around the line centers. This width is sufficiently narrow that potassium atoms with about 10 km sec^{-1} of radial velocity

respect to the sun have emission that are Doppler shifted completely out of the absorption feature. In fact, for a potassium atom moving about Jupiter with Io's circular speed of 17.32 km sec^{-1}, continuum level sunlight is available for resonance scattering over more than half of its orbital path. This is in contrast to a sodium atom in Io's extended atmosphere which has an absorption depth of about 5% of the continuum level and an absorption width sufficiently broad that the full continuum level is note reached even for a Doppler shift corresponding to a radial velocity of 17.32 km sec^{-1} with respect to the sun.

This difference in the shapes of the potassium and sodium solar absorption features will be reflected directly in a different functional dependence, with repsect to the satellite phase angle, of the cloud intensity and the perturbing effects of solar radiation pressure on the cloud. In contrast to this different functional dependence, the maximum magnitudes of the acceleration produced by the solar radiation pressure will in fact be comparable for both potassium and sodium atoms, having a value of about 1.25 cm s^{-1} and 1.36 cm sec^{-1} respectively for a 17.32 km sec^{-1} Doppler shift. These two accelerations correspond respectively to 1.7% and 1.9% of the gravitational acceleration of Jupiter at Io's orbit. In modeling, therefore, the Io potassium cloud should exhibit east-west asymmetries of similar magnitude to those discussed earlier for the sodium cloud by Smyth (1979, 1982).

IV. PROGRESS IN MODELING SATURN'S RING ATMOSPHERE

4.1 Introduction

A hydrogen atmosphere associated with Saturn's rings has been reported from rocket measurements (Weiser, Vitz and Moos, 1977; Weiser and Moos, 1978), from the earth-orbiting Copernicus (Barker et al., 1980) and IUE (Clarke et al., 1981) satellites and from the Pioneer 11 (Judge, Wu and Carlson, 1980) and Voyager 1 and 2 (Broadfoot et al., 1981; Holdberg, 1982) spacecrafts. Analysis of the rocket data by Carlson (1980) suggested that photodissociation of surface water molecules on the icy ring material might be the source of hydrogen for the atmosphere. A preliminary survey of information describing charged-particle sputtering and photon-sputtering of H_2O ice and the chemical products so formed was therefore undertaken to further explore this idea.

In this survey, virtually no information has yet been uncovered to characterize the photo-sputtering process. Measurements for electron and ion sputtering on icy surfaces have, however, been pioneered by L. J. Lanzerotti, W. L. Brown and colleagues at Bell Laboratories in collaboration with R. E. Johnson at the University of Virginia (see Brown et al., 1980). Applying these measurements to the Saturn sytem, Cheng, Lanzerotti and Pirronello (1982) concluded that the relevant ion phase space densities show that the dominant contribution to charged-particle sputtering arises in the vicinity of Saturn's E-ring and the moons Dione and Tethys. The phase space density above the A and B rings is too small to provide a significant source of hydrogen for the ring atmosphere. The authors also noted that the photo-sputtering rate assumed by Carlson (1980) for the nearly maximum tilt angle of the rings with respect to the sun, appropriate for the rocket measurements of Weiser, Vitz and Moos (1977), should decline significantly when the rings are nearly edge-on to the sun, a geometry appropriate to the Voyager observations. The results of the rocket measurement and Voyager UVS measurements are, however, comparable, which led the authors to question the validity of the photo-sputtering mechanisms.

Preliminary efforts in the first year have been initiated to address such apparent discrepancies. A study has therefore been undertaken to investigate the sources, sinks and orbital dynamics of H atoms for the hydrogen ring atmosphere as well as the absorption, re-emission and chemical nature of H_2O icy surfaces. This is viewed as a preliminary and necessary step before developing a serious numerical model for the ring atmosphere. As an initial departure point, effort has been mainly restricted to studying (1) the initial velocity distribution of hydrogen expected from photo-sputtering and (2) the fraction of the liberated hydrogen that is spatially restricted to the near vicinity of the rings.

4.2 Preliminary Study

In the absence of available information for photo-sputtering, a preliminary study was begun to look at the upper limiting energetic case for photo-sputtering of H_2O ice: that of photo-absorption of H_2O vapor by the solar UV radiation. This should be the upper limit case since all binding energy of H_2O molecules with the ice surface and all inelastic absorption of energy by the ice surface are neglected. Results of our survey of this energetically limiting upper case are summarized in Table 3. The results are divided into reactions for four wavelength intervals and the product velocities for H atoms and OH molecules are indicated. The fraction of the total H_2O photoabsorbed for each reaction is also given for both quiet and active sun conditions. For quiet sun conditions, 90.7% of the reactions produce H atoms directly, 3.4% of the reactions produce H_2 molecules and O atoms directly, and 5.9% of the reactions produce various ion products. For the 90.7% of the reactions producing H atoms, 67% have speeds peaked at about 20 km sec^{-1} from reaction 1a, 16.7% have speeds of 30 km sec^{-1} from reaction 2a, 4% have speeds of about 5 km sec^{-1} from reactions 2c, 2d, and 3c, 2.8% have speeds varying between 25 to 35 km sec^{-1} from reaction 3a, and 0.2% have speeds between 0 and 17 km sec^{-1} from reaction 3d. From this it can be concluded that 95.4% of the H atoms directly liberated have velocities between about 20 and 35 km sec^{-1} (2.09 to 6.4 ev), that 4.4% have velocities of about 5 km sec^{-1} (0.13 ev) or less and that 0.2% have velocities between 0 and 17 km sec^{-1} (0 to 1.5 ev).

Table 3. Photoabsorption of Solar UV Radiation by H_2O Vapor

	Wavelength Range	Reaction	Product Velocities (km sec^{-1}) H Atom	Product Velocities (km sec^{-1}) OH Molecule	References	Fraction of Total H_2O Photoabsorbed Quiet Sun	Fraction of Total H_2O Photoabsorbed Active Sun
1.	1357Å < λ < 1960Å	$H_2O + h\nu \rightarrow H + OH(X^2\Pi)$	20	1.2	1, 2, 5, 10	.670	.534
		$\rightarrow H_2 + O(^1D)$	--	--		.007	.005
2.	λ = 1216Å	$H_2O + h\nu \rightarrow H + OH(X^2\Pi)$	30	1.8	3, 4, 5, 6, 7, 10	.167	.269
		$\rightarrow H_2 + O(^1D)$	--	--		.023	.036
		$\rightarrow H + OH^*(A^2\Sigma^+) \rightarrow H + O + H$	≤ 5.0;?	--		.027	.044
		$\rightarrow H + OH(A^2\Sigma^+)$	5.0	0.3		.009	.015
3.	984Å < λ < 1357Å, λ ≠ 1216Å	$H_2O + h\nu \rightarrow H + OH(X^2\Pi)$	25-35	1.2-2.0	3, 4, 5, 6, 7, 10	.028	.021
		$\rightarrow H_2 + O(^1D)$	--	--		.004	.003
		$\rightarrow H + OH^*(A^2\Sigma^+) \rightarrow H + O + H$	4.0-6.0;?	--		.004	.003
		$\rightarrow H + OH(A^2\Sigma^+)$	0-17.0	0-1.0		.002	.001
4.	λ < 984Å	$H_2O + h\nu \rightarrow$ ionization products [H_2O^+, etc.]	--	--	8, 9	.059	.069

The A, B, C and D rings of Saturn are located radially between about 1.0 and 2.3 planetary radii (R_S). For a nominal ring radius of 1.5 R_S, the circular orbital speed of a ring particle is 20.5 km sec^{-1} and it has a period of 2.75×10^4 sec. For an H atom emitted from the ring particle to escape from Saturn's gravitational field, it must have a minimum velocity in the forward direction of motion of 29.0 km sec^{-1} or a velocity vector relative to the ring particle of 8.5 km sec^{-1} (i.e., a kinetic energy of 0.38 ev). For an H atom emitted from the ring particle to collide with Saturn, it must have a minimum velocity in the backward direction of motion of only 2.17 km sec^{-1} (i.e., a kinetic energy of 0.025 ev) relative to the ring particle. It is then clear from the results of Table 3 above that most H atoms produced from water vapor will be lost from the rings by collision with Saturn and gravitational escape from Saturn. In fact, a simple calculation reveals that the fraction of H-atoms that have initial orbits within the radial interval between one and four Saturn radii is only 7%. Subsequent collision with the ring particles of this selected 7% will cause even these H atoms to be rapidly lost through collisions with Saturn. The residence time of an H atom in the torus would under these circumstances be too short to allow a substantial H cloud to be formed for the rings.

If an effective binding energy is assumed for the water ice surface to describe the work function of the surface and all inelastic absorption of energy by the ice surface, the results described above for the pure water vapor case can be generalized and significantly improved. Steady state balances for the number of H atoms in the rings can in fact be established which allow residence times of sufficient lengths to provide the required 8×10^{33} H atoms in the ring atmosphere measured by Weiser et al. (1977) and Weiser and Moos (1978). Even though this appears to be a promising solution for formation of the H atom ring atmosphere, other more difficult questions such as how to limit the abundance of the atomic oxygen ring atmosphere (produced by the photoabsorption reactions of Table 3) below the upper limit of 2.6 Rayleighs set for the 1304 Å lines by the UV measurements of Voyager 1 (Broadfoot et al., 1981) remain to be answered. This and other related issues will continue to be pursued in our further studies during the second program year.

V. REFERENCES

Bagenal, F. and J.D. Sullivan (1981) Direct Plasma Measurements in the Io Torus and Inner Magnetosphere of Jupiter. J. Geophys. Res., 86, 8447.

Barker, E., S. Cazes, C. Emerich, A. Vidal-Madjar and T. Owen (1980) Lyman-Alpha Observations in the Vicinity of Saturn with Copernicus. Ap. J., 242, 383.

Belcher, J.W. (1981) Private communication.

Broadfoot, A.L. et al. (1981) Extreme Ultraviolet Observations from Voyager 1 Encounter with Saturn. Science, 212, 206.

Brown, R.A., C.B. Pilcher and D.F. Strobel (1981) Spectrophotometric Studies of the Io Torus. Preprint of a chapter to appear in Physics of the Jovian Magnetosphere, A.J. Dessler (ed.).

Brown, R.A. and N.M. Schneider (1981) Sodium Remote from Io. Preprint, article submitted to Icarus.

Brown, W.L. et al. (1980) Energy Dependence of the Erosion of H_2O Ice Films by H and He Ions. Nuc. Instr. and Meth., 170, 321.

Carlson, R.W. (1980) Photo-Sputtering of Ice and Hydrogen Around Saturn's Rings. Nature, 283, 461.

Cheng, A.F., L.J. Lanzerotti and V. Pirronello (1982) Charged Particle Sputtering of Ice Surfaces in Saturn's Magnetosphere. Preprint.

Clarke, J.T., H.W. Moos, S.K. Atreva and A.L. Lane (1981) IUE Detection of Bursts of HLYα Emission from Saturn. Nature, 290, 226.

Goldberg, B.A. (1981) Private communication.

Holberg, J.B. (1982) Private communication.

Judge, D.L., F.-M. Wu and R.W. Carlson (1980) Ultraviolet Photometer Observations of the Saturnian System. Science, 207, 431.

Kurucz, R.L. (1982) Private communication.

Murcray, F.J. and R.M. Goody (1978) Pictures of the Io Sodium Cloud. Ap. J., 226, 327.

Pilcher, C. (1980) Transient Sodium Ejection from Io. Bull. Am. Astron. Soc., 12, 675.

Pilcher, C.B. (1981) Private communication.

Pilcher, C.B., J.H. Morgan, J.H. Fertel and C.C. Avis (1981) A Movie of the Io Plasma Torus. Bull. Am. Astron. Soc., 13, 731.

Scudder, J.D., E.C. Sittler, Jr. and H.S. Bridge (1981) A Survey of the Plasma Electron Environment of Jupiter: A View from Voyager. J. Geophys. Res., 86, 8157.

Shemansky, D.E. (1980) Private communication.

Smyth, W.H. (1979) Io's Sodium Cloud: Explanation of the East-West Asymmetries. Ap. J., 234, 1148.

Smyth, W.H. (1982) Io's Sodium Cloud: Explanation of the East-West Asymmetries. II. accepted for publication in Ap. J. (October 15 issue).

Smyth, W.H. and M.B. McElroy (1978) Io's Sodium Cloud: Comparison of Models and Two-Dimensional Images. Ap. J., 226, 336.

Trafton, L. (1975a) Detection of a Potassium Cloud near Io. Nature, 258, 690.

Trafton, L. (1977) Periodic Variations of Io's Sodium and Potassium Clouds. Ap. J., 215, 960.

Trafton, L. (1980) An Explanation for the Alternating North-South Asymmetry of Io's Sodium Cloud. Icarus, 44, 318.

Trafton, L. (1981a) A Survey of Io's Potassium Cloud. Ap. J., 247, 1125.

Trauger, J.T. (1981) CCD Images of the Jovian [SII]-[SIII] Nebula: Photometry and Line Ratios. Bull. Am. Astron. Soc., 13, 730.

Weiser, H. and H.W. Moos (1978) A Rocket Observatoin of the Far-Ultraviolet Spectrum of Saturn. Ap. J., 222, 365.

Weiser, H., R.C. Vitz and H.W. Moos (1977) Detection of Lymanα Emission from the Saturnian Disk and from the Ring System. Science, 197, 755.

VI. REFERENCES FOR TABLE 3

1. Stief, L.J., Payne, W.A. and Klemm, R.B. 1975. J. Chem. Phys., 36, 605.

2. Welge, K.H. and Stuhl, F. 1967. J. Chem. Phys., 16, 2440.

3. Carrington, T. 1964. J. Chem. Phys., 41, 2012.

4. McNesby, J.R., Tanaka, I., and Okabe, H. 1962. J. Chem. Phys., 36, 605.

5. Festou, M.C. 1981. Astron. Astrophys., 96, 52.

6. Slanger, T.G. 1982. Private communications.

7. Lee, L.C. 1980. J. Chem. Phys., 72, 4334.

8. Oppenheimer, M. and Downey, C.J. 1980. Ap. J. Lett., 241, L123.

9. Hudson, R.D. 1971. Critical reveiw of UV photoabsorption cross sections for molecules of astrophysical and aeronomic interest. Natl. Stand. Ref. Data Ser., Natl. Bur. Stand. (U.S.) 38, 50-52.

10. Okabe, H. 1978. Photochemistry of Small Molecules. John Wiley & Sons, Inc., New York, p. 201-203.

APPENDIX A

IO AND TITAN: SATELLITE ION SOURCES

by

William H. Smyth

presented before the

Jovian/Saturnian Magnetospheric Conference

Applied Physics Laboratory
The Johns Hopkins University
Laurel, Maryland

October 22-24, 1981

Introduction

I will report on modeling of observat ns for UV and optical emissions from extended neutral gas atmospheres of the outer satellites.

Three objectives of this modeling are to better understand the local satellite atmosphere, to better understand the interaction of the satellite and its atmosphere with the magnetosphere, and to better assess the importance of the extended satellite atmosphere as an ion-source for the magnetosphere.

The presentation today will focus only upon the last of these objectives by discussing modeling results for the ion creation rate and the initial spatial distribution of the satellite ion-sources produced by Io's atomic oxygen cloud and by Titan's hydrogen torus.

Io's Oxygen Cloud

The atomic oxygen cloud of Io was discovered by Brown in 1980 by earth-based observations of its emission in the 6300Å oxygen lines.

Slide 1 Our model calculation for the Io oxygen cloud viewed at the mid-point of Brown's measurements is shown in the first slide.

Brightness contours for the 6300Å emission are indicated in Rayleigh and assume a satellite escape flux of 10^{10} atoms $cm^{-2}sec^{-1}$.

Impact of Io plasma-torus electrons with the oxygen atoms determines both the lifetime of the oxygen atoms in the Jovian environment and the brightness of the oxygen atom emissions in the 6300Å lines.

A two-dimensional distribution for the Io plasma-torus electrons was used in the calculation, and reflects the Voyager 1 encounter conditions as determined by the UVS and plasma measurements.

The two locations of Brown's observing aperature are indicated by the shaded rectangles, and his average measured value of 8 ± 4 Rayleighs is in agreement with the model calculation, if a slightly reduced satellite escape flux of 5×10^{9} oxygen atoms $cm^{-2}sec^{-1}$ is adopted.

Slide 2 This produces an ion creation rate of 2×10^{27} ions sec^{-1} having an initial spatial distribution relative to Io, shown in the next slide, as viewed from above the satellite plane.

Note that the ion creation rate is concentrated near Io and mostly outside of its orbit, and also ahead of Io and mostly just inside its orbit.

The outer contour corresponds to an ion creation value of 4.4×10^{5} ions $cm^{-2}sec^{-1}$ while the maximum value at Io corresponds to an ion creation rate of 1.9×10^{7} ions $cm^{-2}sec^{-1}$.

Assuming that equal numbers of sulfur ions would also be produced in a similar manner near Io, and that a plasma instability mechanism could thermalize the newly created co-rotational energies of these ions in about an hour, one would

produce a hot electron source located just ahead of Io's orbital position with an energy input of about 2.6×10^{11} watts or about 14% of the total energy radiated in the UV torus.

This may provide an explanation for the Io-correlated energy source for the plasma torus recently discovered by Sandel from analysis of Voyager UVS data.

Slide 3 In the next slide, the radial distribution of this ion-creation-rate is shown and indicates that ionization of oxygen atoms in the Io plasma torus is unsymmetric about Io's orbital location.

Slide 4 This occurs because the oxygen atom lifetime is radial asymmetry about Io on the centrifugal equation of the plasma torus, as indicated in the next slide.

The oscillation of the Io plasma torus about the satellite plane, which is not included in the present model calculations, will vary the oxygen atom lifetime at Io position by about a factor of 8.

This oscillation will also vary the 6300Å volume emission rate by a factor of about 6, so that the increased lifetime is approximately offset by a decrease in emission rate.

Future model calculations, including the oscillating plasma torus, will refine the present model results.

Titan Hydrogen Torus

Slide 5 A Pre-Voyager model of the Titan hydrogen torus based upon analysis of Lyman-α emissions measured by the Earth-

orbiting Copernicus satellite and by the UV instrument of Pioneer 11 is shown on the next slide.

A spatially uniform charge-exchange lifetime of 5600 hr or 2×10^7 sec and a radial ejection flux of $1\text{-}3 \times 10^9$ H-atoms $cm^{-2}sec^{-1}$ from Titan's exosphere with a mean emission speed of 2.0 km/sec were assumed to calculate the Lyman-α intensity pattern of a few hundred Rayleighs shown.

The model is valid when there are no collisions between cloud atoms.

The torus is nearly symmetric about Saturn except near Titan.

The total height of the torus is about 6 Saturn radii and it has an apparent radial extent from about 8 to 28 Saturn radii.

UV observations of Voyager 1 measured a similar radial confinement of the Titan torus, but gave no indication of its vertical extent.

Slide 6 The corresponding calculated radial distribution of the number of hydrogen atoms lost per 0.1 Saturn Radii per sec because of change exchange is given on the next slide and represents a maximum ion exchange rate of about 2×10^{27} ions sec^{-1}.

The ion exchange rate is peaked at Titan's orbit and extends radially from 12 to 36 Saturn radii. A net ion creation rate of order 1% of these indicated value would be expected from electron impact ionization and photoionization.

Recent Voyager 2 measurements of the Titan-hydrogen torus determined its total vertical extent to be about

12-14 Saturn Radii, about a factor of two larger than the pre-Voyager model results.

Vugraph 1 Comparison of our pre-Voyager model parameters for the Titan torus with new values deduced from preliminary analysis of Voyager 2 UVS and plasma data are indicated on the next viewgraph.

The major revision of the earlier model parameters results from a H-Atom lifetime 5 times larger.

This, however, is offset by an increased torus volume of comparable size so that the effective ion-exchange rates remain about the same, having a value of about 1×10^{27} ions sec^{-1}.

In addition to the improved values of the model parameters, future models for the Titan hydrogen torus should also include the spatially non-uniform lifetime of oxygen atoms introduced inside of 8 Saturn Radii by the E-ring plasma torus and introduced outside of Titan's orbit by the solar-wind-magnetospheric boundary.

Vugraph 2 This is illustrated in the last viewgraph, where the cross-sectional envelope of the Titan hydrogen torus is shown for atom escape speeds of 1.0, 1.5 and 2.0 km/sec.

Furthermore, the validity of the model assumption of no collisions between cloud atoms may be called in question if the flux of H_2 or other molecules emitted by Titan is significantly larger than the deduced hydrogen atom flux of order 1×10^{9} $cm^{-2}sec^{-1}$.

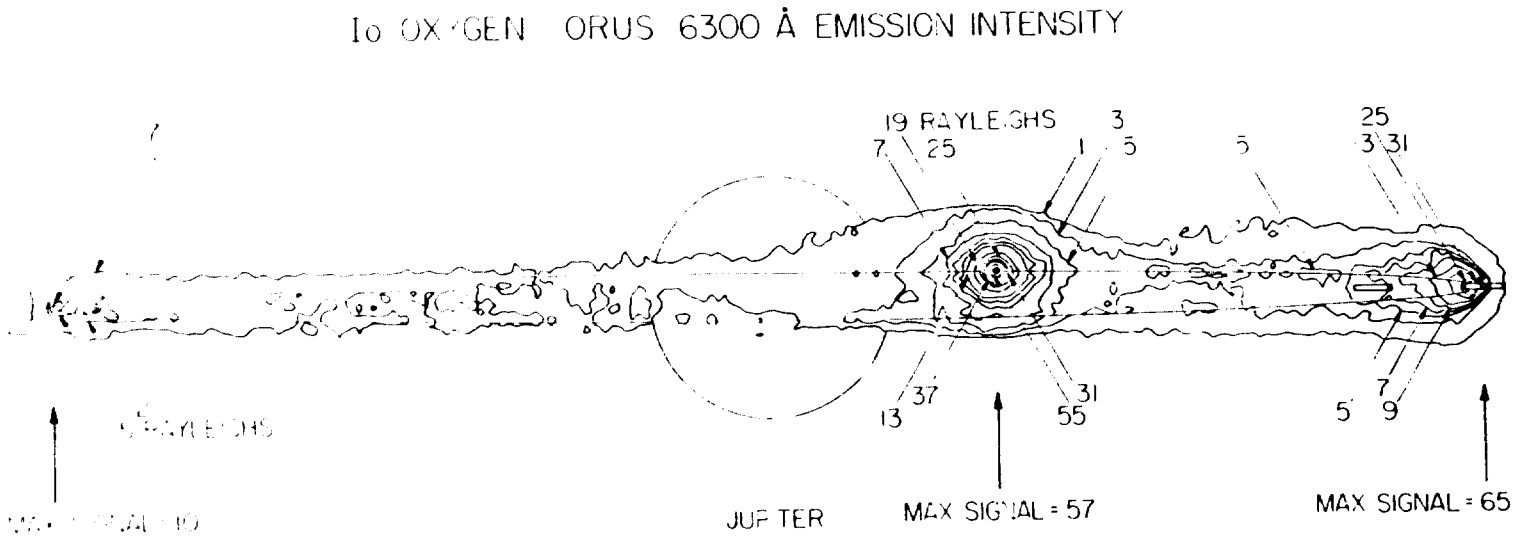

Slide 1

Io: Oxygen Ion Creation Rate

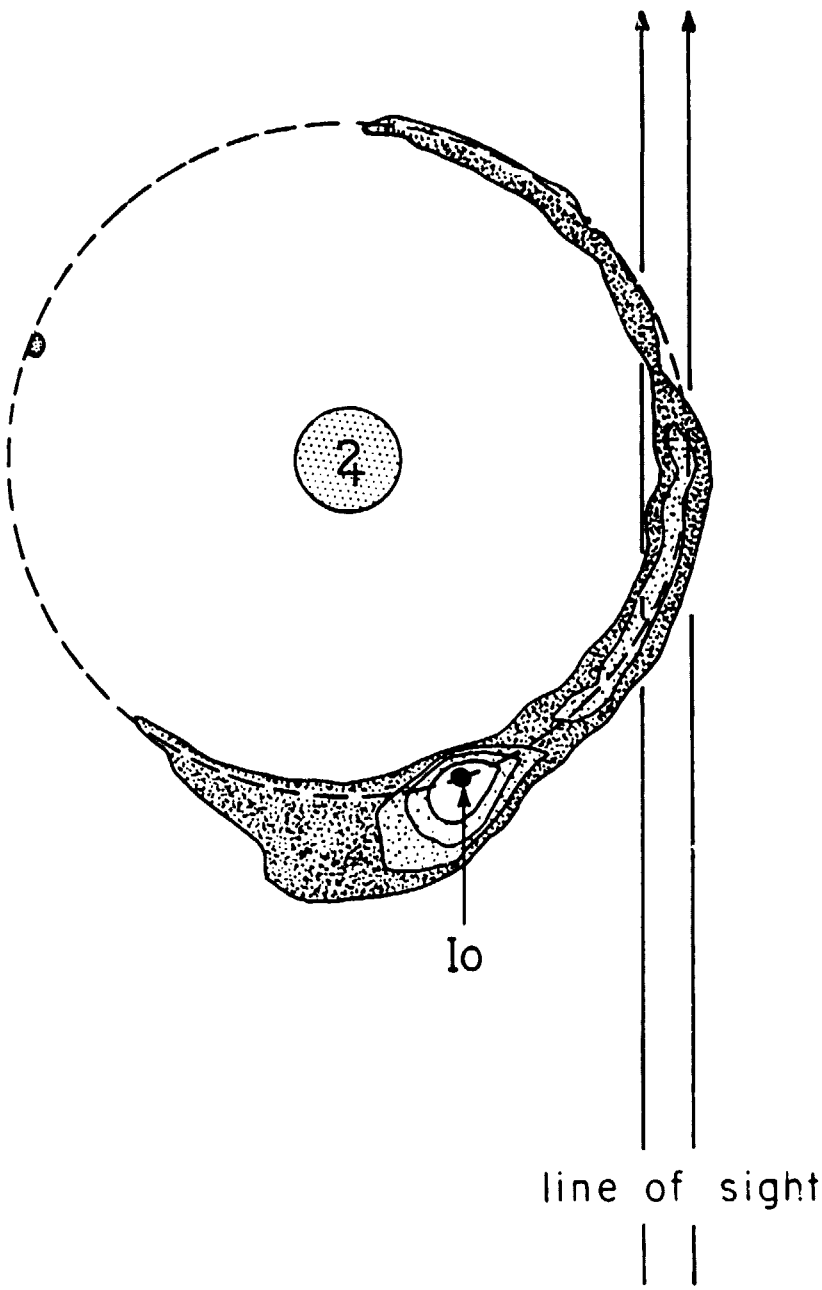

Slide 2

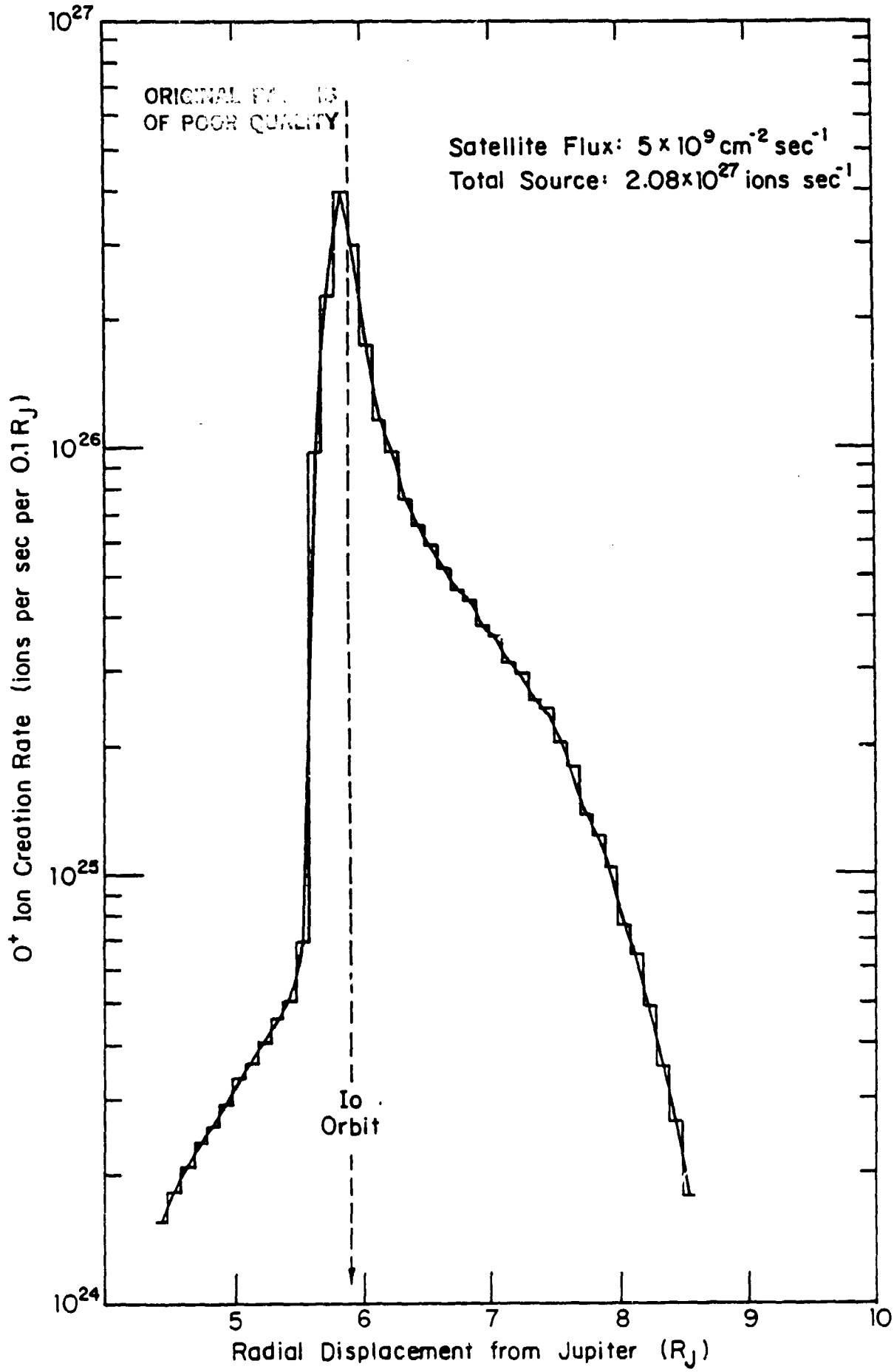
ORIGINAL PAGE IS
OF POOR QUALITY
Satellite Flux: 5 x 10^9 cm^-2 sec^-1
Total Source: 2.08x10^27 ions sec^-1
Io
Orbit
O+ Ion Creation Rate (ions per sec per 0.1 RJ)
Radial Displacement from Jupiter (RJ)
10^27
10^26
10^25
10^24
5
6
7
8
9
10

Slide 3

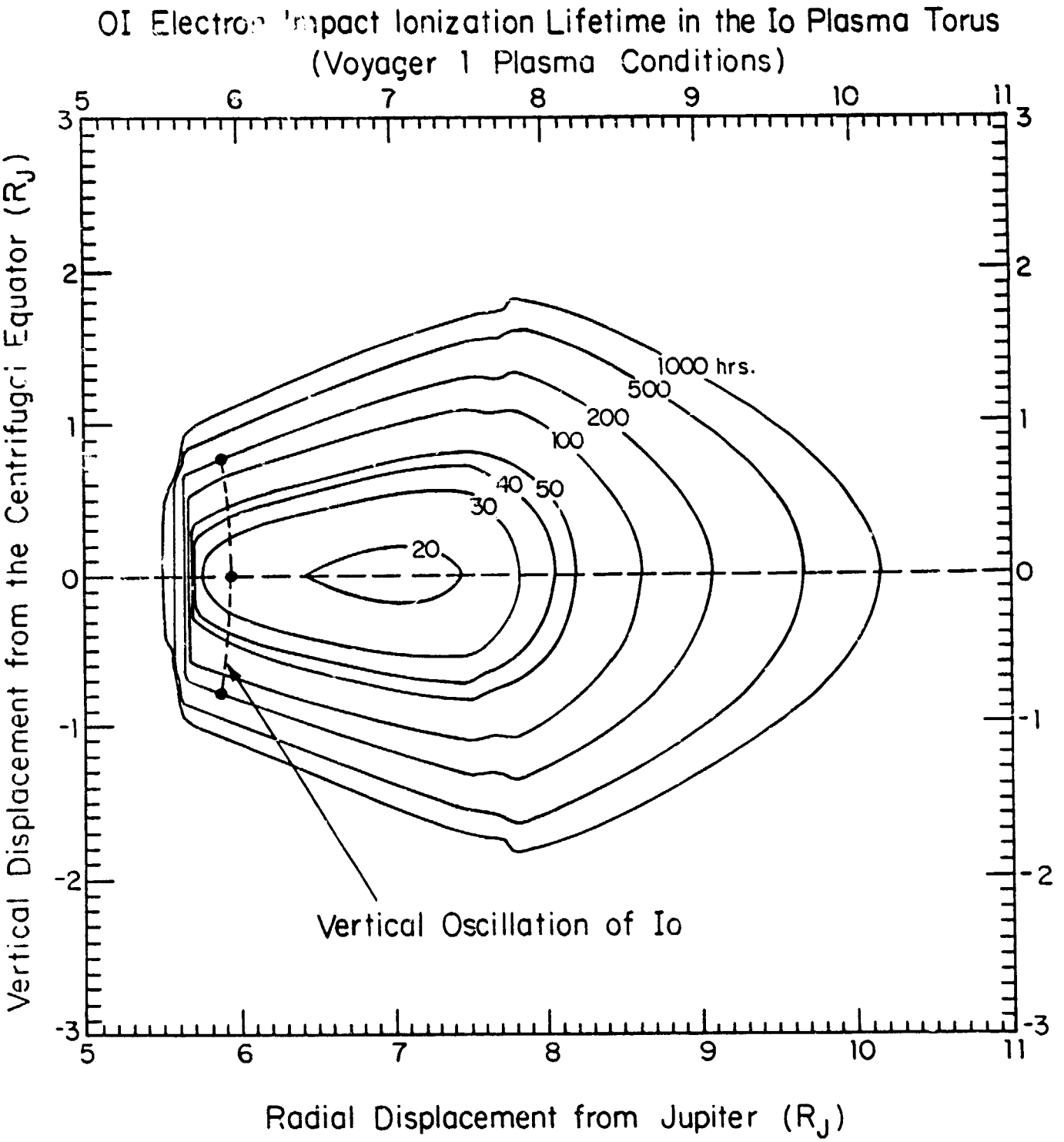

Slide 4

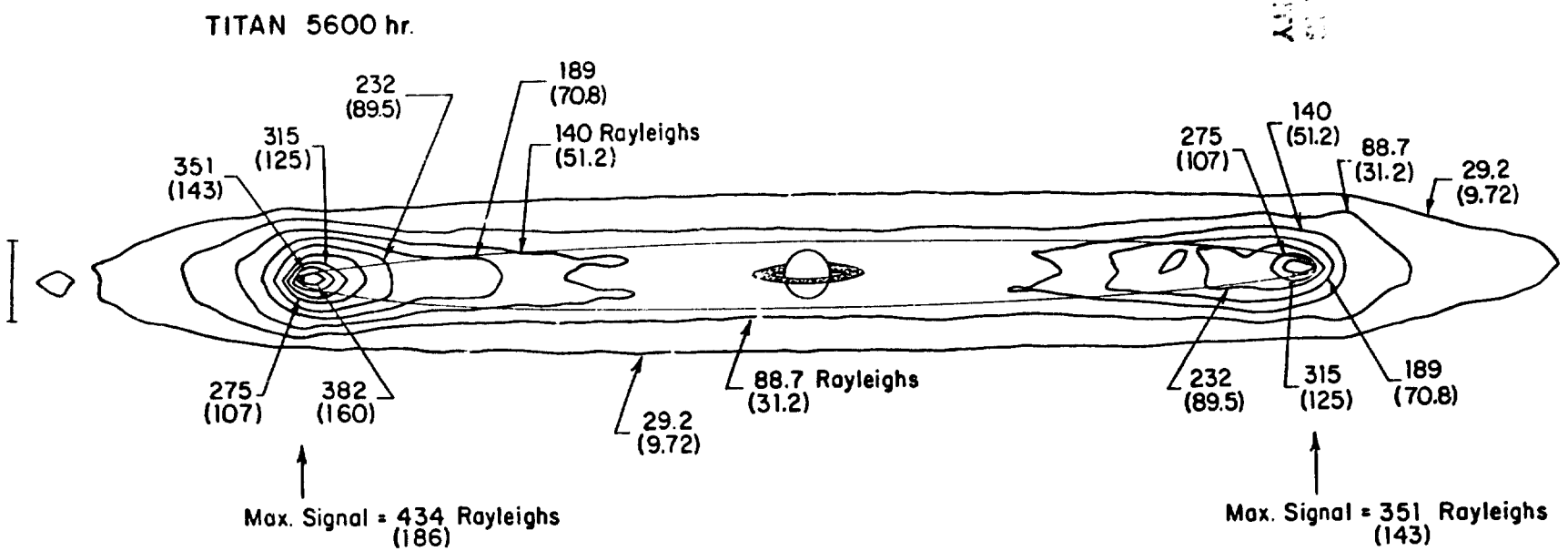

Slide 5

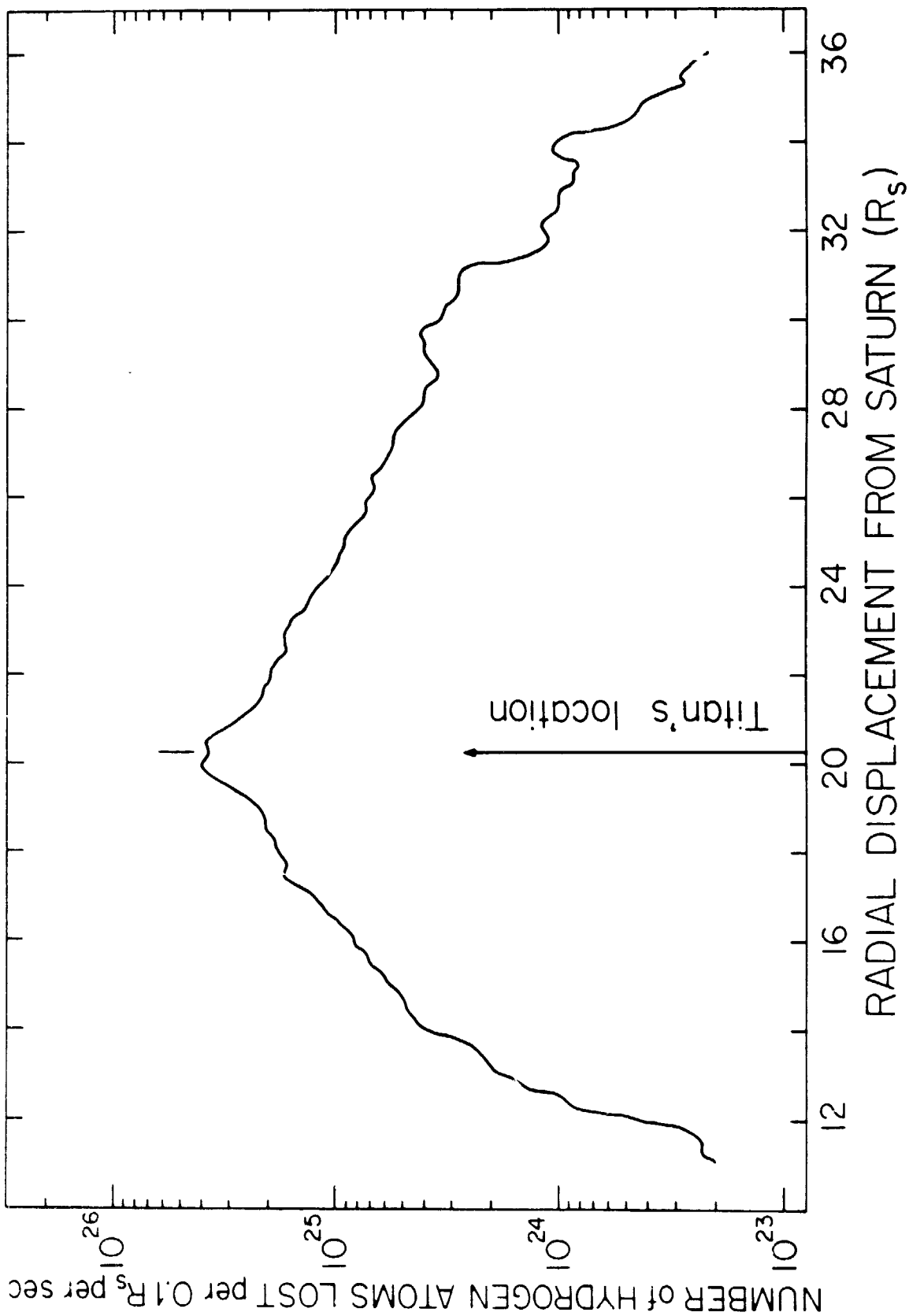

Slide 6

TITAN HYDROGEN TORUS

Parameter	Voyager 2 Observations	Pre-Voyager Model	Comment
H-Atom Lifetime	1×10^{8} sec	2×10^{7} sec	factor 5 too small
Mean Exospheric Emission Speed	2.6 km sec^{-1}	2.0 km sec^{-1}	slightly larger
(Atom Escape Speed)	(1.9 km sec^{-1})	(1.0 km sec^{-1})	(half height of obs cloud)
H-Atom Satellite Flux	1.4×10^{9} cm^{-2} sec^{-1}	$1\text{-}3 \times 10^{9}$ cm^{-2} sec^{-1}	similar
Total Number Torus Atoms	1.07×10^{35} atoms	$1.5\text{-}4.6 \times 10^{34}$ atoms	factor 2-7 too small
Ion Exchange Rate	1.07×10^{27} ions sec	$0.77\text{-}2.3 \times 10^{27}$ ions sec^{-1}	similar

Viewgraph 1

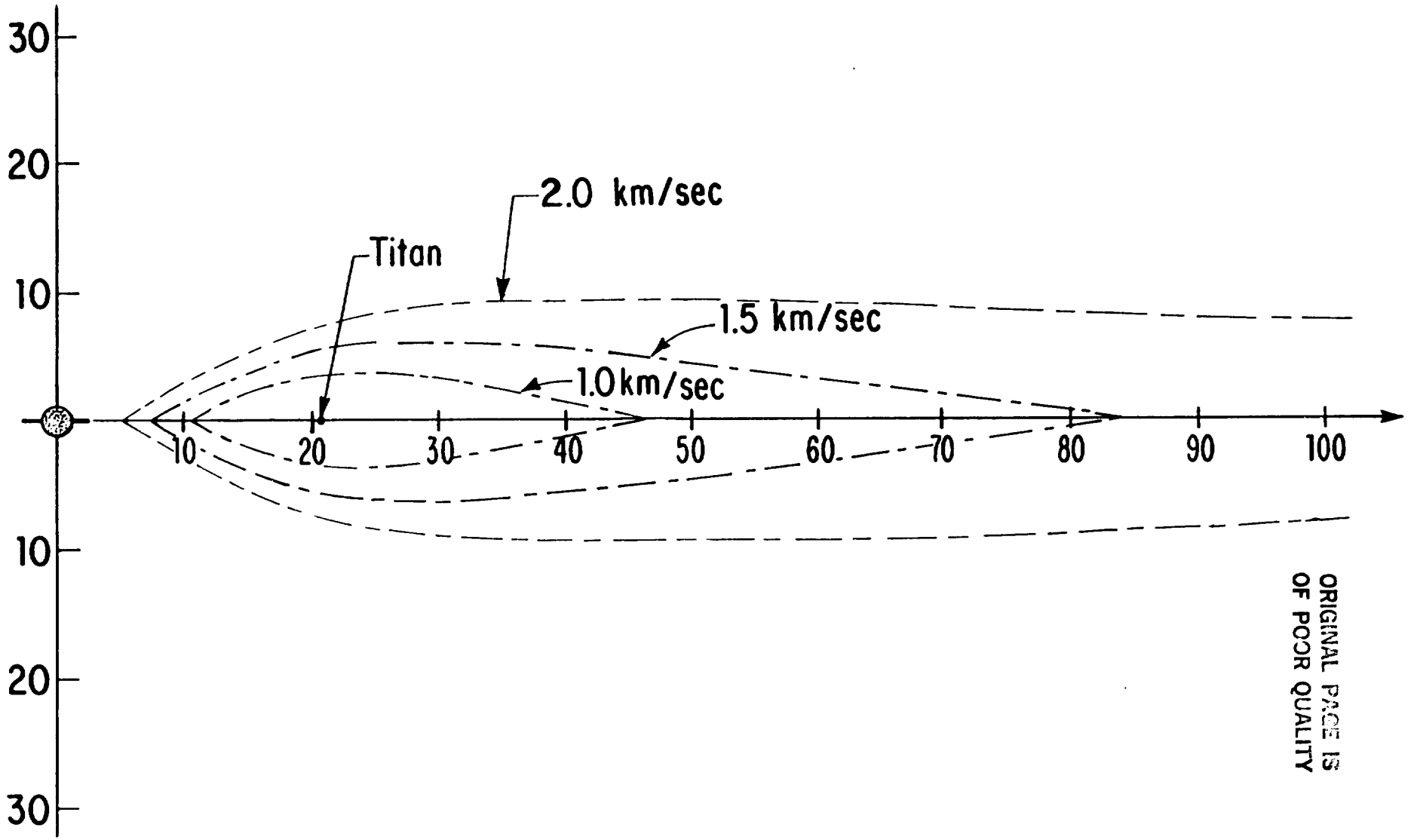

Viewgraph 2

APPENDIX B

IO'S SODIUM CLOUD: EXPLANATION OF THE EAST-WEST ASYMMETRIES. II

William H. Smyth

Atmospheric and Environmental Research, Inc.
840 Memorial Drive
Cambridge, Massachusetts 02139

submitted for publication in
The Astrophysical Journal

ABSTRACT

A new model has been developed for the sodium cloud of Io to describe its geocentric phase-angle dependent interaction with the solar radiation pressure arising from resonance scattering of sunlight in the D_1 and D_2 lines. Solar radiation pressure, acting along the Sun-Jupiter line, introduces an asymmetrically directed force into the otherwise cylindrically-symmetric gravitational three-body problem as described in a coordinate frame moving with the orbital motion of the satellite about Jupiter. The new model was developed to more quantitatively explore the hypothesis, originally presented in Paper I (Smyth, 1979), that solar radiation pressure provides a mechanism for explaining the east-west asymmetry in the cloud shape discovered by Goldberg et al. (1978) and the east-west cloud intensity asymmetry discovered by Bergstralh et al. (1975). From more recent observational data (Goldberg et al., 1980; Goldberg, 1981) these separately reported asymmetries now appear to be interrelated. Model calculations presented here confirm the original hypothesis and uncover explicit mechanisms for the observed east-west asymmetries. Model results presented for the cloud intensity do not, however, include the spatially and time dependent sodium lifetime produced by the oscillation of the Io plasma torus about the orbital plane of the satellite. Modifications to these results anticipated upon inclusion of the Io plasma torus in the model are, however, discussed and represent the only

major improvement to this model required before proper inversion of the east-west asymmetry data may be undertaken.

1. Introduction

In an earlier paper (Smyth, 1979; hereinafter referred to as Paper I), an explanation of the observed east-west asymmetries of the Io sodium cloud, based upon the effects of solar radiation pressure, was presented. These asymmetries were discovered by Bergstralh et al. (1975, 1977) and Goldberg et al. (1978) when Earth-based observations of the D-line emissions of the sodium cloud were compared for diametrically opposite satellite geocentric phase angles east and west of Jupiter. In Paper I, the force experienced by sodium atoms as they resonantly scatter sunlight in the D-lines and the ability of this force to alter the cloud atom orbits were explored. Orbit calculations presented showed that this solar radiation pressure produces a significant east-west asymmetry in the cloud shape. First, it acts in a time-dependent fashion, compressing the cloud near eastern elongation and expanding the cloud near western elongation, thereby providing the correct behavior to explain the east-west intensity asymmetry observed by Bergstralh et al. (1975, 1977). Second it causes the sodium cloud to tilt closer to Jupiter when Io is near western elongation that when Io is near eastern elongation, thereby providing an explanation for the east-west cloud shape asymmetry observed by Goldberg et al. (1978). An illustration from Paper I showing these effects is given in Figure 1.

The major objective of Paper I was to demonstrate simply, using orbit calculations restricted to the satellite plane, that solar radiation pressure provides a mechanism which may qualitatively explain the observed east-west asymmetry features. The object of this second paper is to further test this mechanism by providing quantitative and more realistic three-dimensional model calculations for the sodium cloud. To accomplish this, a sodium cloud model, including the inherent time-dependent effects of solar radiation pressure on the orbits of cloud atoms, has been developed. This model represents a substantial modification of the earlier sodium cloud model of Smyth and McElroy (1977, 1978) and is presented in Section 2.

In addition to solar radiation pressure, the actual intensity distribution of the observed sodium cloud will depend upon the initial velocity dispersion of sodium ejected from Io and also upon the spatial and temporal variations of the sodium lifetime in the Jovian environment. Knowledge of this velocity dispersion should be obtained from a careful inversion of the sodium data using the above described cloud model into which the lifetime information and possible ion impact phenomena (Brown and Schneider, 1982) have been properly incorporated. The emphasis of the three-dimensional modeling presented in this paper will not, however, be data inversion. It is rather to provide the preliminary and necessary step of documenting the physical changes that occur in the sodium cloud intensity because of solar radiation pressure.

In this documentation, only the effects of solar radiation pressure on the lower velocity components (0-3 km sec^{-1}) of the actual initial velocity dispersion of the ejected sodium atoms are investigated. These components provide the dominant contribution to the intensity of the near Io sodium cloud. Higher emission velocities (3-15 km sec^{-1}) that do not contribute dominantly to the intensity of the near Io sodium cloud on the sky-plane (Smyth and McElroy, 1978) are not considered here. These higher emission velocities are, however, important, for example, in determining the asymmetric wings of the sodium line profile shape (Trafton, 1975; Trauger et al., 1976; Carlson et al., 1978; Macy and Trafton, 1980), in understanding the peculiar directional features seen by Pilcher (1980) and Goldberg et al. (1980), and in providing a source mechanism for atoms observed in the remote Io sodium cloud (Brown and Schneider, 1982). In this documentation, changes in the cloud density, introduced because sodium atoms are lost in a spatially non-uniform manner by either ion impact or ionization through electron impact with the Io plasma torus, have also not been addressed. These changes represent a further numerical tailoring of the cloud density and D-line intensities within the three-dimensional sodium envelope which has already been altered by the action of solar radiation pressure. It is the altered intensity distribution within this sodium envelope, without this additional numerical tailoring, that is the subject of this paper. The additional effects of this tailoring are currently under

evaluation and will be considered in a future publication. A brief discussion of the anticipated effects of this tailoring is, however, included in the following section.

The discussion of model results for the east-west asymmetries is presented in Section 3 and Section 4. The discussion is divided into two sections for convenience of presentation, not because the results represent two unrelated phenomena. In Section 3, model results for Goldberg's cloud shape asymmetry are discussed, while in Section 4, model results for Bergstralh's intensity asymmetry are discussed. Concluding remarks are presented in Section 5.

2. Sodium Cloud Model

An improved model for the Io sodium cloud is presented for calculation of its density and solar resonance scattered D-line intensities. The model is based upon following the trajectories of many orbits of atoms emitted by the satellite, subject to the combined gravitational fields of Jupiter and Io and the acceleration produced by resonance scattering in the D-lines. This involves numerically solving the equations of motion of each atom in three dimensions, for prescribed initial conditions, and including proper weight factors along each orbit to simulate ionization, elastic collisional loss processes, and excitation phenomena. A description of the equations of motion and the resulting sodium cloud model, when the acceleration produced by solar resonance scattering is not included, was previously considered in detail by Smyth and McElroy (1977, 1978). Similar approaches have also been adopted in other sodium cloud modeling efforts (Matson et al., 1978; Goldberg et al., 1980). In these earlier papers, the motion of sodium atoms in the Io-Jupiter system required numerical solution of the circular restricted three-body problem in three dimensions. The present account provides an extension of these earlier papers by explicitly including the acceleration of sodium atoms produced by solar resonance scattering in the D-lines.

The trajectories of sodium atoms in the improved model are governed by what will be called the modified circular

restricted three-body equations of motion, given as follows:

$$\ddot{x} - 2\dot{y} = \frac{\partial \Phi}{\partial x} + \vec{b} \cdot (\hat{i}_\xi \cos t + \hat{i}_\eta \sin t) \tag{1}$$

$$\ddot{y} + 2\dot{x} = \frac{\partial \Phi}{\partial y} + \vec{b} \cdot (-\hat{i}_\xi \sin t + \hat{i}_\eta \cos t) \tag{2}$$

$$\ddot{z} = \frac{\partial \Phi}{\partial z} + \vec{b} \cdot \hat{i}_\zeta \tag{3}$$

with

$$\Phi(x,y,z) = -\tfrac{1}{2}z^2 + \tfrac{1}{2}[\mu r_1^2 + (1-\mu) r_2^2] + \frac{\mu}{r_1} + \frac{1-\mu}{r_2} \tag{4}$$

$$r_1^2 = (x_1 - x)^2 + y^2 + z^2 \tag{5}$$

$$r_2^2 = (x_2 - x)^2 + y^2 + z^2 \tag{6}$$

$$x_1 = 1 - \mu \tag{7}$$

$$x_2 = -\mu \tag{8}$$

and

$$\mu = \frac{m_1}{m_1 + m_2} \tag{9}$$

$$\vec{b} = b\, \hat{i}_{sun} \tag{10}$$

where b is the acceleration experienced by sodium atoms because of resonance scattering in the D-lines, expressed in dimensionless form. The normal circular restricted three-body equations of motion are recovered when b is equal to zero (see Smyth and McElroy, 1977).

The coordinates (x,y,z) measure the displacement of the sodium atoms with respect to the center of mass of the Jupiter-Io system in units of the constant separation distance between the planet and satellite. Velocities $(\dot{x},\dot{y},\dot{z})$, accelerations $(\ddot{x},\ddot{y},\ddot{z})$ and time t are defined in dimensionless fashion using the reciprocal of the angular frequency for motion of the planet and satellite around their center of mass as a characteristic time. Satellite and planet masses are denoted by m_1 and m_2 respectively.

The coordinates (x,y,z) are defined in a non-inertial frame which rotates in such a manner to maintain the planet and satellite at fixed positions on the x-axis as shown in Figure 2. These rotating coordinates are related to dimensionless inertial frame coordinates (ξ,η,ζ), with right handed unit vectors $(\hat{i}_\xi,\hat{i}_\eta,\hat{i}_\zeta)$, by the transformation

$$\begin{pmatrix} \xi \\ \eta \\ \zeta \end{pmatrix} = \begin{pmatrix} \cos t & -\sin t & 0 \\ \sin t & \cos t & 0 \\ 0 & 0 & 1 \end{pmatrix} \begin{pmatrix} x \\ y \\ z \end{pmatrix} \qquad (11)$$

The inertial frame, also with origin at the center of mass of the Jupiter-Io system, is positioned with its ζ-axis normal to the satellite orbit plane and its ξ-axis in the plane defined by the Earth-Jupiter line and the ζ-axis. For an Earth observer the direction of positive ξ is away from the Earth toward Jupiter when the tilt angle of the satellite plane viewed from the Earth is zero. The unit vector $\hat{i}_{sun}$ is directed away from the sun along the Sun-Jupiter line.

The acceleration b is given by

$$b = (b_1 + b_2) / \left[\frac{G(m_1 + m_2)}{a^2}\right] \qquad (12)$$

where b_1 and b_2 are the contributions to the acceleration of a sodium atom by resonance scattering in the D_1 and D_2 lines respectively, where G is the gravitational constant and a is the constant separation distance between the planet and satellite. The acceleration b is made nondimensional by the characteristic acceleration given in brackets, which is effectively the gravitational acceleration experienced by a sodium atom in circular orbit of radius a about Jupiter. The magnitude of the acceleration b, as discussed in detail in Paper I, is as large as 0.01 to 0.02 and depends upon the radial velocity v of the sodium atom with respect to the sun in the following manner:

$$b_i = \frac{h\nu_i}{m_0 c} J_i \qquad (13)$$

where

$$J_i = \gamma_i(v)\left(\frac{\pi e^2}{m_e c}\right)\left(\frac{\pi F_{\nu_i}}{h\nu_i}\right) f_i R^{-2} \; . \qquad (14)$$

Here $\frac{h\nu_i}{c}$ is the momentum change experienced by a sodium atom of mass m_0 upon absorbing a photon of energy $h\nu_i$ in the D_1 line (i=1) or D_2 line (i=2) and J_i is the corresponding rate at which photons are absorbed. In the expression for J_i, R is the Sun-Jupiter distance in astronomical units, f_i is the oscillator strength of the i^{th} line,

πF_{ν_i} is the solar continuum-level photon energy flux between the D_1 and D_2 lines at R = 1, and $\gamma_i(v)$ is the fraction of this solar continuum flux available to the sodium atom as it is Doppler shifted out of the bottom of the solar D-line Fraunhofer absorption feature by the instantaneous radial velocity v of the sodium atom relative to the Sun. The velocity v is the sum of the radial component of the velocity of the center of mass of the Jupiter-Io system $\vec{u}_{cm}$ and the velocity of the sodium atom $\vec{u}_{atom}$ in the inertial frame with respect to the Sun:

$$v = (\vec{u}_{cm} + \vec{u}_{atom}) \cdot \hat{i}_{sun} \qquad (15)$$

where

$$\vec{u}_{atom} = \sqrt{\frac{G(m_1 + m_2)}{a}} \, (\dot{\xi}, \dot{\eta}, \dot{\zeta}) \qquad (16)$$

and where $(\dot{\xi}, \dot{\eta}, \dot{\zeta})$ is given in terms of (x,y,z) and $(\dot{x}, \dot{y}, \dot{z})$ by differentiation of (11) with respect to t:

$$\begin{pmatrix} \dot{\xi} \\ \dot{\eta} \\ \dot{\zeta} \end{pmatrix} = \begin{pmatrix} -\sin t & -\cos t & 0 \\ \cos t & -\sin t & 0 \\ 0 & 0 & 0 \end{pmatrix} \begin{pmatrix} x \\ y \\ z \end{pmatrix} + \begin{pmatrix} \cos t & -\sin t & 0 \\ \sin t & \cos t & 0 \\ 0 & 0 & 1 \end{pmatrix} \begin{pmatrix} \dot{x} \\ \dot{y} \\ \dot{z} \end{pmatrix} . \qquad (17)$$

The presence of the solar radiation acceleration in the equations of motion (1) - (3) makes the differential

equations explicitly time-dependent in two ways. First there is the obvious explicit time-dependence in equations (1) - (3) introduced because of the changing vector direction of $\vec{b}$ in the (x,y,z) frame. Second, there is the complex time-dependent modulation of the magnitude of the acceleration vector b as described by (13) - (17). The value of b varies more than an order of magnitude and is strongly dependent upon the satellite phase angle through the first term in (17) and is also dependent upon the instantaneous velocity of the sodium atom $(\dot{x},\dot{y},\dot{z})$ relative to Io through the second term of (17). These two sources of explicit time dependence severely complicate the solutions of the equations of motion (1) - (3). The natural circular symmetry of the gravitational problem that exists in the (x,y,z) frame when b = 0 is destroyed, thus causing each atom ejected from Io with a given set of initial conditions to have a different trajectory for each different initial location of the satellite on its circular orbit. This breakdown of the natural circular symmetry of the gravitational problem caused by the introduction of the acceleration b gives rise to east-west differences in the cloud atom orbits discussed in Paper I and provides a mechanism to explain the east-west asymmetries observed in the sodium cloud.

Model calculations of the density and intensity of the sodium cloud are based upon determining the locus and instantaneous velocity of cloud atoms in space resulting from continuous ejection of sodium from Io. This locus of atom positions for each of the individual initial conditions used to

describe this ejection process cannot be obtained by simply integrating the equations (1) - (3) once over the effective lifetime of the atom in the Jovian environment for one orbital location of Io as was accomplished in earlier modeling efforts where b is zero. In the present case, as the satellite is moving around its orbit continuously emitting sodium, the atoms ejected at different satellite orbital locations experience a different force and therefore have different trajectories even though their initial conditions relative to the satellite are identical. The determination of the desired locus of atom positions in the (x,y,z) coordinates and their corresponding velocities therefore must be constructed, for each initial condition, from the solutions of the equations of motion (1) - (3) for a succession of different locations of the satellite along its orbit. The length of the angular section over which these successive solutions are required is determined by the effective lifetime of the sodium atoms. This angular section must also be properly pre-positioned along the satellite orbit to correctly define the cloud history at the time of observation. The number of satellite locations chosen within a given angular sector will be determined by the spatial resolution of the cloud density and intensity required in the model calculation.

The equations of motion (1) - (3) may be taken to define a set of coupled first order differential equations which determine the time evolution of $(x,y,z,\dot{x},\dot{y},\dot{z})$. These equations are solved numerically using a fourth order Runge-Kutta method.

The equations (1) - (3) exhibit no integrals of motion. Accuracy of the numerical solution is achieved by using carefully constructed sets of small time steps for integrating each atom orbit. In performing these integrations, properly constructed weight factors along each orbit to simulate ionization, collisional loss processes, and D-line excitations of the sodium cloud atoms may also be calculated and used to compute the column density, D-line intensities, and D-line emission profiles of the cloud.

In the model, the continuous ejection of sodium by Io is described by many orbits of atoms which are initially emitted from a spherical exobase. In the model calculations to follow, the atoms are initially emitted radially from the exobase taken to lie at an altitude of 780 km above the satellite surface. Other non-radial emission cases presently incorporated in the model, such as ejection of sodium atoms from the satellite exobase by a Jupiter magnetospheric wind produced by the relative motion of the Io plasma torus past the satellite, are not considered here. These non-radial emission cases are of importance in studying data describing the asymmetric line profile shape of the sodium D-lines (Trafton, 1975; Trauger, Roesler and Much, 1976; Trafton and Macy, 1977; Carlson et al., 1978), data describing the peculiar directional features of the sodium cloud (Hartline, 1980; Pilcher, 1980; Goldberg et al., 1980) and data describing the elastic ion-neutral collisions near Io that appear to populate the remote Io sodium cloud (Brown and Schneider, 1982). For model calculations considered in this paper, the exosphere

has 1298 source points distributed uniformly over the spherical surface. Radial emission of atoms from this exobase will, however, be restricted to monoenergetic ejection of sodium from the inner hemisphere of the satellite which involves only 685 of these source points. The inner hemisphere is selected, since earlier modeling efforts (Smyth and McElroy, 1978; Matson et al., 1978; Macy and Trafton, 1980) have shown it to be the dominant emission hemisphere to explain the two-dimensional intensity features of the sodium cloud. This assumption of inner hemisphere emission may actually reflect the presence of an extreme spatial asymmetry in the lifetime sink for sodium in the Io plasma torus to be discussed later.

Ionizations of the sodium atoms along their orbits in the following model calculations are limited to the simplest description of a constant cutoff lifetime of 20 hours and no attempt is made, as discussed earlier, to address the more complex spatially non-uniform and time-dependent tailoring of the sodium cloud produced by its interaction with the Io plasma torus. The lifetime of sodium atoms in the Io plasma torus, based upon Voyager 1 data for the plasma density (Bridge, Sullivan and Bagenal, 1980; Bagenal and Sullivan, 1981) and for the electron temperature deduced from UVS (Shemansky, 1980) and in situ measurements (Scudder, Sittler and Bridge, 1981), is presented in Figure 3 and seen to be as small as about one hour near the satellite. This small lifetime value for sodium atoms is in marked contrast to the lifetime estimates of 15 to 20 hours (Smyth and McElroy, 1978)

and 28 hours (Matson et al., 1978) obtained from earlier modeling efforts and to the 20 hour value to be adopted here. In these earlier modeling studies, where no spatial variation of the sodium lifetime was assumed, the value of the lifetime was essentially determined by properly modeling the spatial extent of the forward sodium cloud observed in Earth-based measurements.

With the presence of the plasma torus since established, it is now clear that the forward extent of the sodium cloud is determined by ionization of these cloud atoms upon their secondary encounter with the plasma torus, somewhat ahead of Io, which occurs for flight times of order 20 hours (as illustrated in Figure 4). During the first encounter of the cloud atoms with the plasma torus (i.e., as they escape Io initially) the abundance of sodium atoms in the cloud is reduced in a manner which depends critically upon the time history of the atom orbits and their location in the plasma torus, which oscillates about the satellite plane. In Figure 3, the sodium lifetime at Io, for example, varies by a factor of three during this oscillation. This spatial and time-dependent destruction of the sodium density within the 20 hour cloud envelope will not be treated in this paper. The value of 20 hours for the sodium lifetime is adopted, however, in order to preserve the correct dimensions for the forward sodium cloud.

From Figure 4, it is relatively easy, however, to anticipate four effects of including the spatially non-uniform ionization of the Io plasma torus on the model calculations

presented here. First, note that the forward cloud, as determined by the Io plasma torus, will be significantly more elongated for western phase angles than for eastern phase angles, when cloud images are compared for diametrically opposite satellite locations about Jupiter. This more elongated behavior of the western cloud has been confirmed in recent measurements of Goldberg et al. (1980) and Goldberg (1981). The longer forward cloud in the west and the shorter forward cloud in the east will not, however, be a steady state phenomena, but will be seen as a time-dependent modulation about some mean state with an effective period of about 25 Io rotations or 44.25 days. This longer effective period results because of the non-resonance in the 13 hour period of oscillation (with respect to Io) of the plasma torus about the satellite plane, and the 42.5 hour period of the asymmetric behavior of the sodium cloud introduced by the solar radiation pressure.

Second, note that the density and D-line intensity of the diametrically opposite sodium clouds in Figure 4 will be modified differently by the Io plasma torus. The actual flight times for those sodium atoms which travel along the innermost edge of the forward east and west clouds, attaining a radial distance of 5.5 Jupiter radii at their second encounters with the plasma torus, are about 28 and 24.8 hours respectively. This difference will produce a relative density enhancement in this portion of the forward east cloud. On the other hand, the outer edge (closest to the satellite orbit)

of the forward cloud in the east will experience a relative density reduction because of its more complete overlap with the Io plasma torus. The trailing portion of the east cloud outside of the satellite orbit will, however, have a relative density enhancement. This will occur because solar radiation pressure causes the atoms in this portion of the east cloud to move radially out of the plasma torus more rapidly than the corresponding portion of the west cloud, as can be seen in Figure 4. The net effect may well be an overall relative density enhancement for the east cloud, but further model computations are clearly required. These density changes will, of course, be time-dependent and may likely cause the mean east-west cloud shape asymmetry calculated in this paper to be modified in such a way as to affect the predicted value of the east critical phase angle more than the predicted value of the west critical phase angle. The critical phase angles are the satellite phase angles for which the sodium cloud on the sky plane appears to be distributed approximately symmetrically about Io.

Third, note that because of the first ionization encounter of the forward cloud atoms with the Io plasma torus, the ratio of the sodium density and D-line intensities very near Io to that in the forward portion of the cloud will be larger than in the present calculation. This will cause any east-west intensity asymmetry effects that originate near Io to be enhanced and will also require that a larger flux of sodium atoms be emitted from Io in order to properly populate the

elongated portion of the forward cloud. Brown (1981) has estimated that this increased sodium flux may be as large as 6×10^{26} atoms sec^{-1}.

Fourth, note that the extreme radial asymmetry of the sodium lifetime shown in Figure 3 and Figure 4 will provide a larger survival lifetime for sodium which moves inside the satellite orbital radius and populates the forward cloud, and a much smaller survival lifetime for sodium which moves outside the satellite orbital radius and populates the trailing cloud. This suggests that the apparent non-uniformity in the atom emission flux of sodium from Io (i.e., ejection from the inner hemisphere of Io with a spatially uniform lifetime of about 20 hours) deduced from earlier studies (Smyth and McElroy, 1978; Matson et al., 1978; Macy and Trafton, 1980) might actually be explained by a symmetric ejection flux from Io with the very asymmetric spatial sink of the plasma torus. Comparison of two-dimensional sodium cloud images with very preliminary results calculated with our model including a non-oscillating plasma torus suggests, however, that the asymmetric sink is not strong enough. Inclusion of the oscillating motion of the plasma torus in the model may, however, provide the necessary time-average enhancement of the sink asymmetry needed to allow calculations assuming symmetric emission from Io to be consistent with the observed sodium images.

Initial velocities of atoms emitted from the satellite exobase in the following model calculations are limited to

values less than 3 km sec^{-1} for two reasons. First, the mean emission velocity associated with the formation of the forward portion of the near Io cloud, for the brightness levels greater than about 1000 Rayleighs viewed by Goldberg et al. (1978), is 2.6 km sec^{-1} (Smyth and McElroy, 1978). This value of the mean emission velocity determines the inclination angle of the forward cloud, the angle between the central axis of the forward cloud and the tangent line to the satellite orbit at Io (see Figure 1) which was shown in Paper I to be modulated by solar radiation pressure. Larger mean emission velocities produce mean inclination angles that are too large whereas smaller mean emission velocities produce mean inclination angles that are too small. Second, sodium atoms ejected from the exobase, with emission velocities slightly in excess of the satellite escape speed at that altitude, provide the dominant contribution to the D-line intensity in the spatial region close to Io observed by Bergstralh et al. (1975, 1977). This behavior is illustrated in Figure 5 where the relative D_2 intensity contribution to their 3 x 8 arc sec slit centered on the satellite is shown for monoenergetic model calculations, excluding solar radiation pressure, with emission velocities ranging from 1.8 km sec^{-1} to 10 km sec^{-1}. The low velocity of 2.0 km sec^{-1} dominates since atoms with this emission velocity move very slowly with respect to Io upon escape. Lower emission velocities have a larger ballistic component and contribute less, whereas higher emission velocities move much more rapidly away from Io and contribute less.

3. Model Results: Goldberg's Cloud Shape Asymmetry

The sodium cloud has been observed by Goldberg et al. (1978) to exhibit an east-west asymmetry in the spatial distribution of the D-line intensities (i.e., in the cloud shape) with respect to the geocentric orbital phase angle of the satellite. Their observations showed that the observed intensity pattern of the cloud, which is its projection on the sky plane, did not produce a mirror image for satellite orbital phase angles separated by 180 degrees. To initially quantify and characterize one of the differences observed in comparison of these east and west cloud images, the critical phase angles were selected as parameters. The cloud exhibits two critical phase angles which occur for those satellite phase angles where the sodium cloud on the sky plane appears nearly symmetric about Io as the satellite approaches either the eastern or western elongation points of its orbital (i.e., 90 degrees or 270 degrees, respectively).

The first estimates of the eastern and western critical phase angles were originally reported by Goldberg et al. (1978) as 65 degrees and 230 degrees respectively. These values were defined quantitatively by measuring, from their two-dimensional cloud images, the integrated intensities seen in two simulated slits located 9 arc sec on either side of Io, and subsequently by determining that satellite phase angle for which the ratio of the two slit intensities was

unity. This method led to a rather well defined value for the critical phase angle in the west, but to a rather ill defined value in the east due to scatter. The less distinct behavior of the data in the east seemed to reflect a fundamental east-west difference in the sodium cloud, not a difference in the quality of the east and west data. Later estimates made with additional observations (Goldberg, 1979) indicated that the critical eastern phase angle might even be as large as 70 to 75 degrees. This then suggested that in the east the central axis of the forward sodium cloud was inclined only about 15 to 20 degrees with respect to the line drawn tangent to the satellite orbit at Io, whereas in the west this inclination angle was about 40 degrees. The sodium cloud would then have an east-west phase lag asymmetry of about 20 to 25 degrees.

The accuracy of these estimates for the east and west critical phase angles and hence for the east-west phase lag asymmetry has been, however, somewhat difficult to determine with exactness from the data of Goldberg et al. (1978) and Goldberg (1979), since changes in the apparent cloud geometry during their 2 to 3 hour long integrations correspond to orbital angles of 17 to 25 degrees and reduce the spatial resolution of their cloud images. To rectify this situation, Goldberg (1981) has recently made several new measurements using an improved instrument with an integration time of about 10 minutes. His preliminary analysis of these new measurements, based upon visual comparisons, indicates that

the western critical phase angle is distinct and occurs near 235 degrees, whereas the eastern critical phase angle is significantly less distinct and occurs somewhere in the angular interval from 55 to 70 degrees. The exact value of the east-west phase lag asymmetry at present, therefore, remains undetermined and may or may not be as large as initially suggested. The one significant east-west asymmetric cloud feature that does occur both in these new measurements and in their older observations is the obvious presence of a distinct critical western phase angle and the noticeable visual absence of a distinct critical eastern phase angle. Quantitative analysis of existing data and acquisition of new data will be required to determine more accurately the critical eastern phase angle and to understand possible variations of its value introduced by both the oscillating Io plasma torus and non secular variations in the local plasma. Further analysis of these data should also be useful in identifying and characterizing other salient features of the east-west cloud distibution asymmetry, such as the greater elongation of the forward portion of the sodium cloud observed for western phase angles by Goldberg et al. (1980) and Goldberg (1981). To provide a step forward, based upon our current understanding, modeling analysis in this section will be restricted to exploring and documenting the east-west phase lag asymmetry introduced by the solar radiation pressure, excluding the spatially non-uniform and time-dependent ionization of sodium atoms by the Io plasma torus.

The preliminary results of calculations in the satellite plane, originally presented in Paper I and repeated here in Figure 1, demonstrate that solar radiation pressure in the D-lines causes the envelope of the sodium cloud to behave in a manner similar to the observations of Goldberg et al. (1978). Changes in the cloud shape in Figure 1 suggest an east-west phase lag of about 15 degrees. It is clear, however, that such an estimate is only preliminary and that the actual three-dimensional distribution of sodium atoms within the cloud envelope must be calculated in order to determine a more accurate phase lag angle. Suitable three-dimensional model calculations for this purpose are presented below.

Three-dimensional model calculations, illustrating the effects of solar radiation acceleration on the D_2 intensity distribution of the sodium cloud viewed parallel to the satellite plane, are given for satellite phase angles of 55 and 235 degrees in Figure 6 and Figure 7, respectively. In these model calculations, which may be compared directly with the simpler results of Figure 1, sodium was emitted radially from the inner hemisphere of Io's exobase (2600 km radius) with a velocity of 2.6 km sec^{-1} and with a cutoff lifetime of 20 hours in the Jovian environment. Each outer contour value is 916 Rayleighs for a surface flux of 10^8 atoms cm^{-2} sec^{-1}, with contours spaced by 367 Rayleighs, increasing inward toward Io. The results of Figure 6 and Figure 7 show that changes in the D_2 intensity pattern of the sodium cloud are not very sensitive to the illumination angle of the sun rel-

ative to the Earth-Jupiter line of sight. The sun angle (i.e., its phase angle plus 180 degrees) is confined to values between about 168 and 192 degrees as the earth moves about the Sun. For a sun angle of 180 degrees, the Earth-Jupiter line of sight and the Sun-Jupiter axis of Figure 1 are identical. For a satellite phase angle of 55 degrees, note that in Figure 6 the effect of solar radiation is to rotate the central axis of the forward elongated sodium cloud further away from Jupiter as anticipated in the results of Figure 1. With solar radiation acceleration included in the model calculation, the inner edge of the cloud (right portion) in Figure 6 is therefore closer to Io while the outer edge (left portion) is extended further from Io. For a phase angle of 235 degrees, note that in Figure 7 the solar radiation pressure has effectively rotated the sodium cloud axis more toward Jupiter, as anticipated in Figure 1. With solar radiation acceleration included, the outer edge of the cloud (right portion) in Figure 7 is therefore closer to Io while the inner edge of the cloud (left portion) clearly reveals that the axis of the forward elongated sodium cloud has already begun to swing through our line of sight.

The model calculations of Figure 6 and Figure 7 indicate that solar radiation pressure introduces an east-west phase lag asymmetry into the spatial distribution of the sodium cloud. This can be illustrated more clearly as follows. In the absence of solar radiation acceleration, model calculations of the D_2 intensity pattern of the sodium cloud for

diametrically opposite satellite phase angles are presented in Figure 8, where the sun angle is 180 degrees and the other model parameters and contour levels are the same as in Figure 6 and Figure 7. Note that the east and west intensity patterns are effectively mirror images of each other, and that the axis of the forward elongated cloud can be seen to swing through our line of sight at a phase angle of about 55 degrees in the east and 235 degrees in the west, yielding no phase lag. The observed changes in the intensity pattern of the cloud with satellite phase angle are almost completely due to the changing geometric viewing perspective of the cloud projected onto the plane of the sky. In Figure 9, the D_2 intensity patterns of the sodium cloud, where the effects of solar radiation acceleration have been included, are presented for the identical diametrically opposite satellite phase angles, model parameters and contour levels used in Figure 8. Near eastern elongation, note that the outer contour of the sodium cloud appears symmetric about Io near a satellite phase angle of between 60 and 65 degrees, whereas near western elongation the cloud appears symmetric at a phase angle of 230 degrees. This produces an east-west phase lag asymmetry between 10 and 15 degrees. If, on the other hand, the distribution of the D_2 intensity <u>within</u> the outer contour in Figure 9 is used as a criterion, approximate symmetry occurs for a phase angle of 65 degrees in the east and 235 degrees in the west. This produces an east-west phase lag asymmetry that is also about 10 degrees. Note that in Figure 9, the passage of the forward cloud axis

through our field of view is much less less distinct in the east than in the west. This makes it more difficult to accurately determine the eastern critical satellite phase angle, a persistent characteristic noted in the observational data of Goldberg et al. (1978, 1980) and Goldberg (1979, 1981).

The results in Figure 8 and Figure 9 are calculated under the assumption of a monoenergetic emission velocity of 2.6 km sec^{-1}. Results for lower emission velocity components that would be included if a more realistic initial emission velocity distribution were adopted have also been calculated. For emission velocities of 2.0 km sec^{-1}, 2.2 km sec^{-1} and 2.4 km sec^{-1}, the intensity patterns on the sky plane are again essentially mirror images, in the absence of solar radiation pressure, when the east and west clouds are compared for diametrically opposite satellite phase angles. The critical phase angles increase with decreasing emission velocity, having a value, in the absence of solar radiation pressure, in the east between 55 and 60 degrees for an initial velocity of 2.4 km sec^{-1} and a value of about 60 degrees for initial velocities of both 2.2 km sec^{-1} and 2.0 km sec^{-1}. With solar radiation pressure included, these model calculations have the same general east-west character as the results presented in Figure 9. Based upon an outer contour criterion, the critical eastern phase angle is about 65 degrees for the emission velocities of 2.4 km sec^{-1} and below, while the critical western phase angle is between 230 and 235 degrees. This provides an east-west phase lag asymmetry

of about 10-15 degrees. Based upon a criterion for a symmetric distribution of intensity within the outer contour, the critical eastern phase angle is about 70 degrees while the critical western phase angle is about 235 degrees for emission velocities of 2.4 km sec^{-1} and lower, producing a 15 degree east-west phase lag asymmetry.

Model results for emission velocities of 2.2 km sec^{-1}, 2.4 km sec^{-1} and 2.6 km sec^{-1} are compared in Figure 10 and Figure 11 for diametrically opposite phase angles east and west of Jupiter. These D_2 intensity images include the effects of solar radiation pressure and are calculated for the same contour levels, emission conditions, and lifetime conditions chosen in Figures 6-9. As the emission velocity decreases, the cloud is more closely confined near Io and provides a rapidly increasing intensity near the satellite. The exact east and west critical phase angles and corresponding east-west phase lag asymmetry predicted from these model calculations will therefore depend to some extent upon the shape of the initial velocity distribution. From the above calculations, however, it is clear that a phase lag of about 10 to 15 degrees would be present even if an initial velocity distribution were adopted. For such an adopted distribution, the passage of the cloud through its eastern critical phase angle would also appear to occur slower than the passage of the cloud through its western critical phase angle. The critical phase angle in the east should be within the angular range from 55 to 70 degrees, while in the west it should be between 230 and 235.

The presence of a distinct critical western phase angle and of a significantly less distinct critical eastern phase angle in the observations of Goldberg (1981) suggests that the non-uniform ionization of sodium introduced by the Io plasma torus oscillating about the satellite plane may tailor and modify, but will not eliminate, the basic characteristics of the east-west cloud distribution asymmetry illustrated by the model calculations in this section. Further quantitative analysis of the data acquired in the 1980-1981 apparition by Goldberg (1981) is warranted. Such analysis should also provide important information for modeling the alternating north-south asymmetry discovered by Trafton and Macy (1975) and discussed further by Trafton (1980).

4. Model Results: Bergstralh's Intensity Asymmetry

The sodium cloud has been observed by Bergstralh et al. (1975, 1977) to exhibit an east-west asymmetry in its absolute intensity. In their observations, the D-line intensities of the sodium cloud were measured as a function of phase angle through a 3" x 8" slit centered on the satellite with the long dimension of the slit oriented approximately perpendicular to the projection of Io's orbital plane. This observational geometry is illustrated in Figure 12. The long dimension of the slit is only slightly larger than the diameter of the Lagrange sphere of Io, within which the gravitational field of the satellite dominates the planetary gravitational field. The spatial region of the cloud sampled by the slit is therefore composed of a mixture of the dense sodium that likely exists within the Lagrange sphere and the somewhat less dense sodium that occurs, along the line of sight, in the foreground and background of this sphere. In this spatial region, sodium atoms emitted from the Io exobase with velocities very near the satellite escape speed are expected to provide the dominant contribution to the slit intensity as shown earlier in Section 2 and in Figure 5.

The D-line intensities of the cloud, measured through this observing slit, were shown by Bergstralh and colleagues to be correlated with Io's orbital position around Jupiter. This correlation made it possible for them to identify resonance scattering of sunlight by sodium atoms as the dominant

excitation mechanism for the cloud. In addition, the measured intensity of the cloud with the satellite east of Jupiter was shown, in their initial paper (Bergstralh, Matson, and Johnson, 1975) to be consistently about 50% greater than the measured intensity with the satellite west of Jupiter. In their second paper (Bergstralh et al., 1977), which included additional observations and a presentation of more select data, this east-west intensity asymmetry was more accurately estimated to be 20 to 25%.

In Paper I, this intensity asymmetry was associated with the ability of solar radiation pressure to compress the east cloud and expand the west cloud envelope, as illustrated in Figure 1. To investigate more fully how solar radiation pressure provides a mechanism to explain this intensity asymmetry, a number of three-dimensional model calculations have been performed and are presented here. The D_1 and D_2 intensities seen through a 3" x 8" slit centered on Io have been calculated as a function of both the satellite phase angle and the initial speed of sodium atoms emitted from the inner hemisphere of Io's exobase. In all of these model computations, the two-dimensional distributions of both the column density and the intensity of the cloud on the sky pla as well as the shape of the sodium D-line profiles, were simultaneously calculated, both excluding and including solar radiation pressure, to understand more fully the basic phenomena.

Model calculations for the relative D_2 intensity seen through the 3" x 8" viewing slit, taken here to have nominal dimensions of 9×10^3 km by $2,4 \times 10^4$ km, are presented in Figure 13 and compared with the observations of Bergstralh et al. (1975). The relative D_2 intensity of the model calculations is shown as a function of the satellite phase angle for four different monoenergetic emission velocities spanning the range from 2.0 km sec^{-1} to 2.6 km sec^{-1}. In each monoenergetic model calculation, the same number of atoms were emitted from Io's exobase. These relative intensities were calculated for sodium atoms emitted from the inner hemisphere of the exobase and include the shadow effect of the disk of Io blocking the cloud behind it. The tilt angle of the satellite plane is assumed to be zero relative to the observer. The sun, observer and Jupiter are assumed to be along the same straight line. Intensities calculated for a satellite-plane tilt angle of a few degrees differ only slightly.

The model calculations of Figure 13 clearly show that solar radiation pressure introduces a large east-west intensity asymmetry for the initial emission velocity of 2.0 km sec^{-1} and a somewhat less pronounced asymmetry for the 2.1 km sec^{-1} emission velocity. Only a small asymmetry is present for the higher emission velocities of 2.4 km sec^{-1} and 2.6 km sec^{-1}. The maximum intensity of the 2.0 km sec^{-1} results is 4.38 times larger than the 2.6 km sec^{-1} results in the east and 3.48 times larger in the west. The relative D_2 intensities for the different velocities in

Figure 13 have a maximum value near 60 degrees in the east and near 230 degrees in the west. In both the east and west, these peak intensities correspond to the enhancement of the sodium cloud density produced by the forward portion of the cloud as it passes through the line of sight of the viewing slit. The peak intensity is larger and more pronounced for the lower emission velocities since the forward cloud is then much more narrow and is much more tightly confined near Io. This spatial behavior of the forward cloud, in the absence of solar radiation pressure, was discussed earlier by Smyth and McElroy (1977), who at that time noted a similarity between their calculated column density peaks and the peaks in the data of Bergstralh et al. (1975). This similarity is also present in the model results of Figure 13, although before an accurate comparison can be made with the observations, the additional modifications introduced by the spatially non-uniform lifetime of the Io plasma torus must be included in the model calculations.

The east-west ratio of the relative D_2 intensity for the 2.0 km sec^{-1} and 2.1 km sec^{-1} emission velocities is presented in Figure 14, where the results of including and excluding the effects of Io's shadow are both indicated. For an emission velocity of 2.0 km sec^{-1} the ratio provides a minimum east-west asymmetry of 17 percent over most of the angular range when the shadow is included, and at a 70 degree phase angle the ratio has a peak value of over 1.8. The 2.1 km sec^{-1} ratio is less pronounced, but still provides a sig-

nificant east-west asymmetry over much of the phase angle interval. The general qualitative behavior of the D_2 intensity ratio exhibited in Figure 14 can be simply understood in terms of the action of solar radiation pressure upon the orbits of sodium atoms. This qualitative explanation will now be discussed in some detail to clarify both the nature of the physical effects involved and the contribution of the phase-lag asymmetry phenomena to the intensity asymmetry.

In Figure 14, the D_2 intensity ratio is greater than unity for east/west phase angles in the range from 0/180 to 40/220 because the column density of the east cloud in the viewing slit is larger than that of the west cloud by approximately 20% for an emission velocity of 2.0 km sec^{-1}. The radial velocity v of most sodium cloud atoms with respect to the sun is larger, however, in the west cloud than in the east cloud, for this phase angle interval, so that the D_2 intensity ratio is reduced somewhat from this column density ratio through the factor $\gamma_i(v)$ in equation (14). This larger velocity of sodium atoms in the west cloud is also evident in sodium line profiles when model results are compared for diametrically opposite satellite phase angles. For an east/west phase angle near 50/230 in Figure 14, the D_2 intensity of the west cloud in the viewing aperature has reached its maximum value, because of the phase lag asymmetry alignment of the forward cloud. The east cloud, however, reaches its maximum D_2 intensity value of about 10 degrees later and

maintains intensity values near this maximum level over a longer phase angle interval, beyond its peak, than does the west cloud (see the model calculation in Figure 13). This gives rise in Figure 14 to the dramatic increase in the D_2 intensity ratio within the east/west phase angle range from 50/230 to 120/300, and to the asymmetric slope of the D_2 intensity ratio about its peak value located at a phase angle of 70/250.

For larger east/west phase angles between 120/300 and 165/345, the D_2 intensity ratio decreases and eventually becomes less than unity. In this angular range, most atoms now seen in the viewing slit are near Io and not in the forward cloud. Solar radiation pressure, in this angular range, so acts on these cloud atoms to elevate the column density of the west cloud by as much as 18% for the 2.0 km sec^{-1} emission velocity and as much as 4% for the 2.1 km sec^{-1} emission velocity. In the west cloud, the radial velocity v of most atoms with respect to the sun is also enhanced over the east cloud and, through the factor $f_i(v)$ in equation(14), causes the D_2 intensity ratio to be reduced even further.

The significant enhancement of the calculated column density of the east cloud relative to the west cloud within the phase angle range 0/180 to 40/220 in Figure 14, may be attributed to two factors. The first one is that solar radiation pressure produces an east cloud that is spatially more tightly confined near Io and hence has elevated densities.

The second and more important factor is that solar radiation pressure modifies the escape process of atoms from Io so that the total number of atoms within the east cloud is larger. This modification of the escape process is also largely responsible for the elevation of the column densities of the west cloud relative to the east cloud within the east/west phase angle range from 135/315 to 170/350.

With regard to the first factor, the density enhancements of the east cloud and the density reductions of the west cloud within the phase angle range 0/180 to 40/220 in Figure 14 are more pronounced for atom emission velocities near 2.0 km sec^{-1}. This occurs because many of these atoms, shortly after emission from the exobase, experience a near balance between the effective gravitational field of Jupiter and Io. This near balance causes the relative magnitude of the solar radiation acceleration experienced by the sodium atom to be favorably amplified. The vector direction of the solar radiation acceleration, being oppositely oriented in the east and west cloud, then asymmetrically and somewhat abruptly alters the orbits of the cloud atoms. Future evolution of these altered atom orbits then produces the density enhancement of the east cloud and density reduction of the west cloud. For the higher emission velocities of 2.4 km sec^{-1} and 2.6 km sec^{-1}, this amplification effect is much smaller since the sodium atoms, moving more rapidly away from Io, spend less time near the Lagrange sphere. The resulting east-west density changes for these higher emis-

sion velocities are therefore much less pronounced and result primarily from the smooth and continuous action of solar radiation pressure over the 20 hour lifetime of the atoms. In the case of the higher emission velocities, the compression of the east cloud and the expansion of the west cloud, as shown in Figure 1, are, in fact, to first order compensated by the column integration along the line of sight and contribute little to the intensity asymmetry.

With regard to the second and more important factor, the ability of solar radiation pressure to modulate the total number of sodium atoms within the cloud occurs essentially for those emission velocities near 2 km sec^{-1} where the escape of atoms is energetically possible only from a limited surface area of the satellite exobase. This energetically possible area of the exobase defines the window in the Lagrange sphere surrounding Io through which the atoms escape. It is this effective exospheric area, from which the emitted atoms are able to escape from the satellite, that is modulated by the action of solar radiation.

The Lagrange window in Io's orbital plane for atoms emitted from the exobase of the satellite has been discussed, in the absence of solar radiation pressure, by Smyth and McElroy (1977). One of their illustrations is shown in Figure 15 for radial emission velocities of 1.8 km sec^{-1}, 2.0 km sec^{-1} and 3.0 km sec^{-1}. For a 1.8 km sec^{-1} velocity, the Lagrange window is closed except near the center of the inner satellite hemisphere (i.e., at 180°) and near the

center of the outer satellite hemisphere (i.e., at 0°). The window is preferentially open in this direction because it is the easiest direction for escape of atoms, since the two collinear Lagrange points, L_1 and L_2, nearest to Io lie along the line connecting Io and Jupiter (see Figure 2). For an emission velocity of 2.0 km sec^{-1}, the Lagrange window is closed on a small sector of the leading inner quadrant and a small sector of the trailing outer quadrant of the exobase. For a velocity of 3.0 km sec^{-1}, the Lagrange window is completely open, since all atoms emitted radially from the exobase now have sufficient energy to escape Io regardless of their initial surface location. In the absence of solar radiation pressure, the percentage of atoms emitted from the inner hemisphere of the exobase that do not escape Io is determined from model calculations to be 60.3, 28.6, 9.6, 1.8 and 0.19 for monoenergetic emission velocities of 1.8 km sec^{-1}, 1.9 km sec^{-1}, 2.0 km sec^{-1}, 2.1 km sec^{-1} and 2.2 km sec^{-1}. These percentage values are, of course, independent of the phase angles at which the satellite is observed.

The ability of solar radiation pressure to modulate, as a function of the satellite phase angle, the percentage of atoms not escaping from Io, having been initially emitted radially from the inner hemisphere of the exobase, is illustrated in Figure 16. Model results, where solar radiation pressure has been both included and excluded, are compared for monoenergetic emission velocities of both 2.0 km sec^{-1} and 2.1 km sec^{-1}. The functional behavior exhibited is

essentially similar in nature for both emission velocities. Solar radiation pressure enhances the escape of sodium atoms for smaller satellite phase angles in the east (i.e., between 0 and 68 degrees for 2.0 km sec^{-1} and between 0 and 98 degrees for 2.1 km sec^{-1}) and for large phase angles in the west (i.e., between 208 and 360 degrees for 2.0 km sec^{-1} and between 291 and 360 degrees for 2.1 km sec^{-1}). This behavior accounts, in Figure 14, for the earlier noted enhancement of the column density of the east cloud relative to the west cloud in the east/west phase angle range of 0/180 to 40/220, and of the west cloud relative to the east cloud in the east/west phase angle range of 135/315 to 170/350. The general behavior exhibited by the effect of solar radiation pressure in Figure 16 may also be anticipated on geometrical grounds by simply considering, as a function of the observed phase angle of the satellite, the 20 hour time history of the orientation of the solar radiation acceleration vector and that portion of the inner hemisphere exobase from which atom escape is modulated.

The maximum observed D_2 intensity reported by Bergstralh et al. (1977) using their best data base was 241 k Rayleighs. This was measured for a satellite phase angle near eastern elongation and was determined by assuming that only a 3 x 3 arc second portion of their observing slit was uniformly illuminated. If the complete 3 x 8 arc second slit is considered, this uniform intensity is reduced to about 90 k Rayleighs. If this intensity were produced by the maximum D_2 intensity given

by the 2.0 km sec^{-1} calculation of Figure 13, a satellite flux of order 1×10^8 atoms cm^{-2} sec^{-1} would be required, in agreement with an earlier estimate by Smyth and McElroy (1978). This flux value of 1×10^8 cm^{-2} sec^{-1} will, however, be revised upward, as noted earlier by Brown (1981), upon inclusion in the model calculation of the highly spatially, non-uniform ionization of sodium atoms by the Io plasma torus.

Modification of the results of Figure 13 and Figure 14 by including the presence of the Io plasma torus in the new model calculations may be anticipated on simply geometrical grounds. The forward sodium cloud for an emission velocity of 2.0 km sec^{-1} will be largely confined between the inner and outer radial boundary of the plasma torus, in contrast to the 2.6 km sec^{-1} results illustrated in Figure 4. The continual exposure of this sodium to the ionization of the plasma torus will cause the atom population in the forward cloud to be significantly diminished relative to the atom population near Io. The dramatic increase in the model calculated D_2 intensity ratio in Figure 14 for an east/west phase angle of 70/250, which occurs because of the passage of the forward cloud through the field of view of the observing slit, will therefore be reduced by this ionization of the plasma torus. The extent of this reduction will depend upon the mean plasma conditions, which have been observed to change over a time period of several months (Sandel et al., 1979), and also upon the time modulation of these mean conditions by the oscillation of the Io plasma

torus about the satellite plane. Inversion of the east-west asymmetry data of Bergstralh et al. (1975, 1977) using an improved model, which properly includes these plasma torus effects, may then be expected to lead to meaningful results.

5. Concluding Remarks

A three-dimensional model for Io's sodium cloud incorporating the full effects of solar radiation acceleration associated with solar resonance scattering of atoms in the D_1 and D_2 lines has been developed. The model has been applied to interpret two different but related east-west asymmetries exhibited in the near Io sodium cloud in data obtained from ground-based telescopes. The major objective of the modeling analysis presented was to document the physical changes produced in the sodium cloud by the solar radiation acceleration, as a function of the satellite phase angle, and to further clarify beyond the efforts of Paper I, how these changes provide an explanation of the observed east-west asymmetries. Model results presented did not include the effects of spatially non-uniform and time variable interactions of cloud atoms with the Io plasma torus. Anticipated modifications of these results by the plasma torus were, however, discussed and are expected to introduce quantitative rather than qualitative changes. The development of an improved model to include the plasma torus in a quantitative fashion is currently in progress.

Model results for the observed east-west cloud shape asymmetry of Goldberg et al. (1978, 1980) and Goldberg (1979, 1981) were presented in Section 3. These results, calculated for different monoenergetic emission velocities, reproduced the correct phase angle behavior of the observations, indicating a distinct critical phase angle in the west between

230 and 235 degrees and a significantly less distinct critical phase angle in the east between 55 and 70 degrees. These results suggest an east-west phase lag asymmetry of 10 to 15 degrees. The general behavior of the cloud shape asymmetry and the value of the phase lag asymmetry predicted by the model calculations are not critically dependent upon the exact distribution of the emission velocities between 2 km sec^{-1} and 3 km sec^{-1} (the velocity range which contributes most dominantly to the intensity of the near Io cloud), because these effects depend primarily upon the simple geometrical orientation of Io's orbit and the solar radiation force vector.

Model results for the observed east-west intensity asymmetry of Bergstralh et al. (1975, 1977) were presented in Section 4. Intensity contributions seen through their 3 x 8 arc sec viewing slit centered on Io were shown to be dominated by atoms with emission velocities less than about 3 km sec^{-1}, with the most important contribution occurring for an emission velocity of 2 km sec^{-1}, a value very near the satellite escape speed at the exobase. Model results near 2.0 km sec^{-1} provide a distinct east-west intensity asymmetry over most of the satellite phase angle range and compare favorably with the observational data. Solar radiation pressure produces this intensity asymmetry by modulating, as a function of satellite phase angle, the size of the Lagrange window through which atoms are able to escape the gravitational field of Io. For atoms with emission veloci-

ties larger than about 2.2 km sec^{-1}, the perturbing effect of solar radiation pressure is not strong enough to modulate the size of the Lagrange window. East-west intensity asymmetry effects for these larger velocities are introduced primarily by the different overlap of the cloud envelope and the Io plasma torus. This overlap is time-dependent, having an overall effective period of 25 Io rotations or 44.25 days, with the mean results likely favoring a relative increase in the east cloud intensity. Future model calculations including the Io plasma torus are, however, definitely needed to clarify this situation.

In summary, the model predicted changes in the shape and spatial orientation of the sodium cloud envelope and in the intensity distributions within the evelope, provide a simple explanation for the east-west shape and intensity asymmetries. These results follow directly from the lack of circular symmetry about Jupiter of the forces acting on the cloud atoms. The lack of this circular symmetry is introduced by the presence of the solar radaition force in the model calculations. The identification of the east-west intensity asymmetry in the model calculations with sodium atoms emitted within a somewhat narrow range of the velocities near the satellite escape speed is significant. Careful model inversion of the east-west intensity data should then be sensitive in accurately determining relative weights in the initial emission velocity distribution for the contributing velocity components in the 1.8 km sec^{-1} to 2.2 km

sec^{-1} velocity interval. This analysis would be somewhat complementary to the inversion of the two-dimensional intensity data for the east-west cloud shape asymmetry seen on the sky plane, which is primarily sensitive to the emission velocities between 2 km sec^{-1} and 3 km sec^{-1}, and to the line profile data of the sodium cloud, which is particularly sensitive to higher emission velocities, up to 15 km sec^{-1} or 20 km sec^{-1}. A consistent and simultaneous analysis of all three types of sodium data should provide the necessary overlapping constraints to deduce the real initial velocity distribution function for sodium atoms escaping from Io.

ACKNOWLEDGEMENT

The author would like to thank B. A. Goldberg for helpful discussions and comments. Appreciation is also expressed to H. S. Bridge, J. D. Sullivan and F. Bagenal who provided the two-dimensional density information and to D. E. Shemansky who provided the electron temperature information for the Io plasma torus used in Figure 3 to calculate the electron impact ionization lifetime of sodium. This research was supported by the Planetary Atmospheres program of the National Aeronautics and Space Administration under grants NASW-3174 and NASW-3387. Acknowledgement is also made to the National Center for Atmospheric Research, which is sponsored by the National Science Foundation, for the computing time used in model computations.

REFERENCES

Bagenal, F. and Sullivan, J.D. (1981) J. Geophys. Res., 86, 8447.

Bergstralh, J.T., Matson, D.L. and Johnson, T.V. (1975) Ap. J. Lett., 195, L131.

Bergstralh, J.T., YOung, J.W., Matson, D.L. and Johnson, T.V. (1977) Ap. J. Lett., 211, L51.

Bridge, H.S., Sullivan, J.D. and Bagenal, F. (1980) private communications.

Brown, R.A. (1981) Cospar 1980 Space Research, XXI, Pergamon, Oxford (article in press).

Brown, R.A. and Schneider, N.M. (1982) Sodium Remote from Io. Icarus (article in press).

Carlson, R.W., Matson, D.L., Johnson, T.V. and Bergstralh, J.T. (1978) Ap. J., 223, 1082.

Goldberg, B.A., Carlson, R.W., Matson, D.L. and Johnson, T.V. (1978) Bull. AAS, 10, 579.

Goldberg, B.A., Mekler, Yu, Carlson, R.W., Johnson, T.V. and Matson, D.L. (1980) Icarus, 44, 305.

Goldberg, B.A. (1979) private communication.

Goldberg, B.A. (1981) private communication.

Hartline, B.K. (1980) Science, 208, 384.

Macy, W. and Trafton, L. (1980) Icarus, 41, 131.

Matson, D.L., Goldberg, B.A., Johnson, T.V. and Carlson, R.W. (1978) Science, 199, 531.

McFarland, R.H. (1965) Phys. Rev., 139, A40.

McFarland, R.H. and Kinney, J.D. (1965) Phys. Rev., 137, A1058.

Pilcher, C. (1980) Bull. AAS, 12, 675.

Sandel, B.R. et. al. (1979) Science, 206, 962.

Scudder, J.D., Sittler, E.C., Jr. and Bridge, H.S. (1981) J. Geophys. Res.. 86, 8157.

Shemansky, D.E. (1980) private communication.

Smyth, W.H. and McElroy, M.B. (1977) Planet. Space Sci., 25, 415.

Smyth, W.H. and McElroy, M.B. (1978) Ap. J., 226, 336.

Smyth, W.H. (1979) Ap. J., 234, 1148.

Trafton, L. (1975) Ap. J. Lett., 202, L107.

Trafton, L. and Macy, W., Jr. (1975) Ap. J. Lett., 202, L155.

Trafton, L. and Macy, W., Jr. (1977) Ap. J., 215, 971.

Trafton, L. (1980) Icarus, 44, 318.

Trauger, J., Roesler, F. and Münch, G. (1976) Bull. AAS, 8, 468.

Zapesochnyi, I.P. and Aleksakhin, I.S. (1968) Zh. Eksp. Teor. Fiz., 55, 76. [also, Soviet Physics JETP, 28, 41 (1969)].

FIGURE CAPTIONS

Figure 1 East-West Changes in the Sodium Cloud. Calculations performed in Paper I for the solar radiation perturbed cloud shape, indicated by the shaded area, and for the unperturbed cloud shape, indicated by the dashed boundary, are compared for diametrically opposite satellite phase angles. The shape of the cloud is the envelope formed by atoms, emitted from Io in the satellite plane, after 20 hours of flight time.

Figure 2 Dimensionless Coordinate System for the Modified Circular Restricted Three-Body Problem in Io's Orbital Plane. The locations of the five classical Lagrange points at L_1, L_2, L_3, L_4 and L_5, the satellite at x_1, and the planet at x_2 in the (x,y)-plane are indicated.

Figure 3 Sodium Electron Impact Ionization Lifetime in the Io Plasma Torus. The lifetime calculation is based upon the measured cross-section by McFarland (1965), McFarland and Kinney (1965) and Zapesochnyi and Aleksakhin (1968). For the plasma data, referenced in the text, the two-dimensional common temperature model of

C-2

Bagenal and Sullivan (1981) was selected to describe the electron density.

Figure 4 Interaction of the Sodium Cloud and the Plasma Torus. The spatially-projected overlap in the satellite plane of the Io plasma torus with the solar radiation perturbed cloud shape (solid boundary with heavy shading) and with the unperturbed cloud shape (heavy dashed boundary) of Figure 1, is indicated for the diametrically opposite satellite phase angles. The cloud shape illustrates the envelope of sodium atoms after 20 hours of flight time.

Figure 5 Relative D_2 Intensity in the Bergstralh Slit. The relative contribution to the solar resonance scattered D_2 intensity seen in the observing slit of Bergstralh et al. (1975, 1977) as determined by monoenergetic model calculations for the sodium cloud, excluding the effects of solar radiation pressure, is shown as a function of the emission velocity of sodium atoms from the inner exobase (2600 km radius) of Io for a satellite phase angle of 77.6 degrees. For each emission velocity, the same number of atoms were emitted from the exobase and a simple constant cut off lifetime of 20 hours was assumed.

Figure 6 Effects of Solar Radiation Pressure in the East Cloud. Calculated D_2 intensity contours of the sodium cloud are compared, with and without the effects of solar radiation pressure, for the indicated phase and sun angles. The outer dashed lines are for reference in comparing the left and right boundaries, and the center dashed line is for vertical alignment of the satellite location.

Figure 7 Effects of Solar Radiation Pressure in the West Cloud. See legend to Figure 6.

Figure 8 East-West Comparison of the Sodium Cloud. Model calculations for the D_2 intensity contours of the sodium cloud, excluding the effects of solar radiation pressure, are shown for diametrically opposite satellite phase angles east and west of Jupiter. No east-west phase lag asymmetry is evident. See text for discussion.

Figure 9 East-West Comparison of the Sodium Cloud. Model calculations for the D_2 intensity contours of the sodium cloud, including effects of solar radiation pressure, are shown for diametrically opposite satellite phase angles east and west of Jupiter. A distinct east-west phase lag asymmetry is evident. See text for discussion.

Figure 10 Dependence of the Sodium Cloud on Emission Velocity. Model calculated D_2 intensity contours for the sodium cloud, including solar radiation pressure effects, are shown for diametrically opposite satellite phase angles and compared for emission velocities of 2.2 km sec^{-1}, 2.4 km sec^{-1} and 2.6 km sec^{-1}. See text for discussion.

Figure 11 Dependence of the Sodium Cloud on Emission Velocity. See legend to Figure 10.

Figure 12 Observational Slit for the Intensity Asymmetry Measurements. The rectangular observational slit of Bergstralh et al. (1975, 1977), centered on Io, is shown in relation to the sodium cloud, the satellite orbit and the planet.

Figure 13 Comparison of Observation and Model Results for the East-West Intensity Asymmetry. The observations of Bergstralh et al. (1975) are compared to model calculations for the relative D_2 intensity seen through their rectangular viewing slit. Model calculations for four different monoenergetic values of the emission velocity are shown. See text for discussion.

Figure 14 Model Results for the East-West Intensity Ratio. The east to west D_2 intensity ratio of Figure 13 is shown as a function of the east to west phase angles for emission velocities of 2.0 km sec^{-1} and 2.1 km sec^{-1}.

Figure 15 Lagrange Window in Io's Orbital Plane for Atoms Emitted from the Exobase of the Satellite. Io, surrounded by its exobase (the dashed circle), is shown as depicted in an original illustration of Smyth and McElroy (1977). The radial coordinate indicates the flight time of an atom emitted radially from the exosphere at the angular orientation about the satellite shown. Upon capture by Io, the 5° angular-resolution radial sector containing that orbit is blackened for all later time. Ballistic orbits are indicated for a capture time of 50 hr. For greater capture times, blackening indicates that atoms, initially on an escape trajectory, have been recaptured because of a close encounter with Io.

Figure 16 Solar Radiation Pressure Modulation of the Sodium Atom Escaping from Io. The percentage of sodium atoms not escaping Io, which are emitted uniformly and at a constant rate from the inner hemisphere of the satellite exobase with monoenergetic emis-

sion velocities of 2.0 km sec^{-1} and 2.1 km sec^{-1}, are compared as a function of the Io phase angle for model calculation excluding (dashed curve) and including (solid curve) the effects of solar radiation pressure. See text for discussion.

William H. Smyth

Atmospheric and Environmental Research, Inc.

840 Memorial Drive

Cambridge, Massachusetts 02139

Figure 1

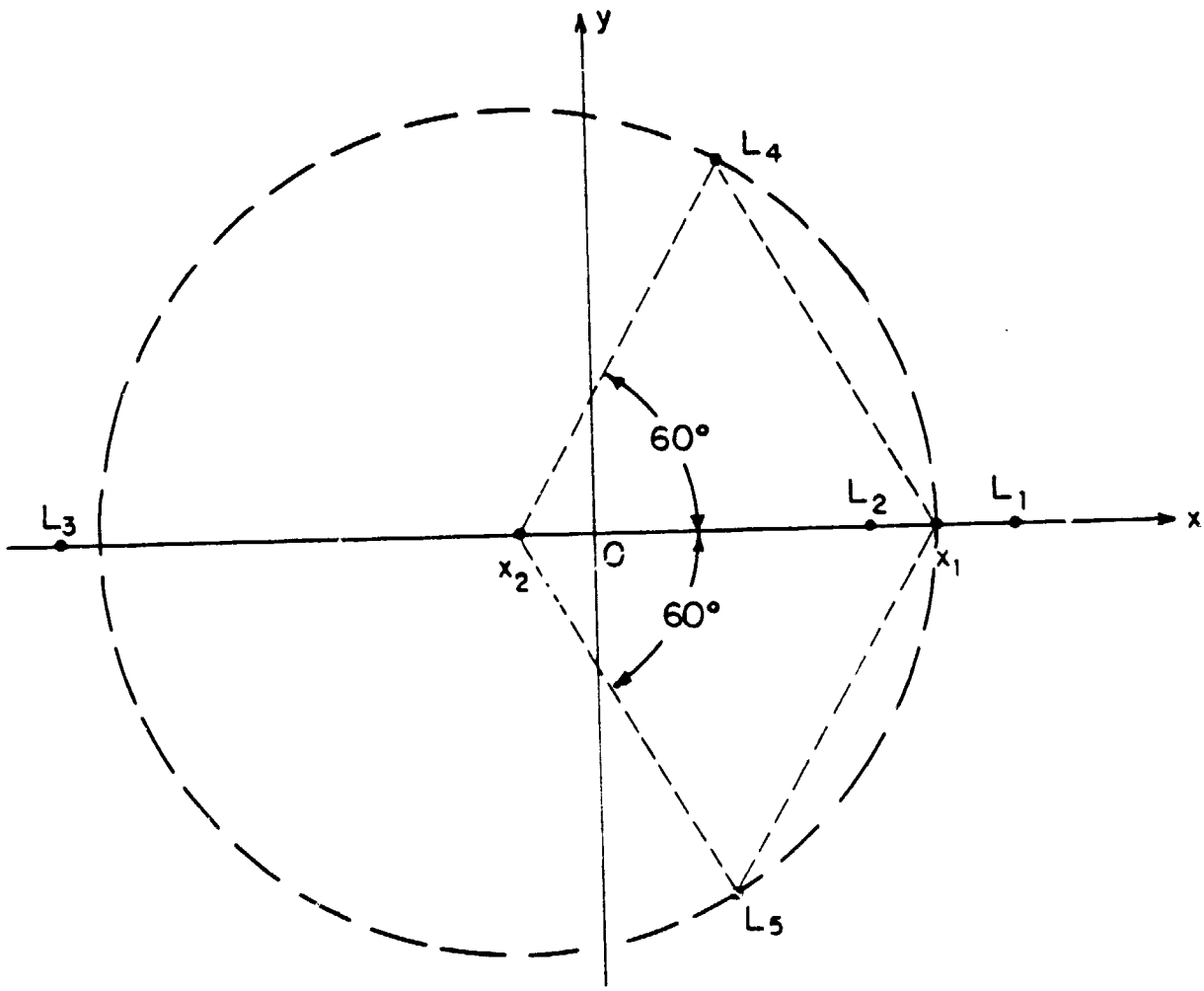

Figure 2

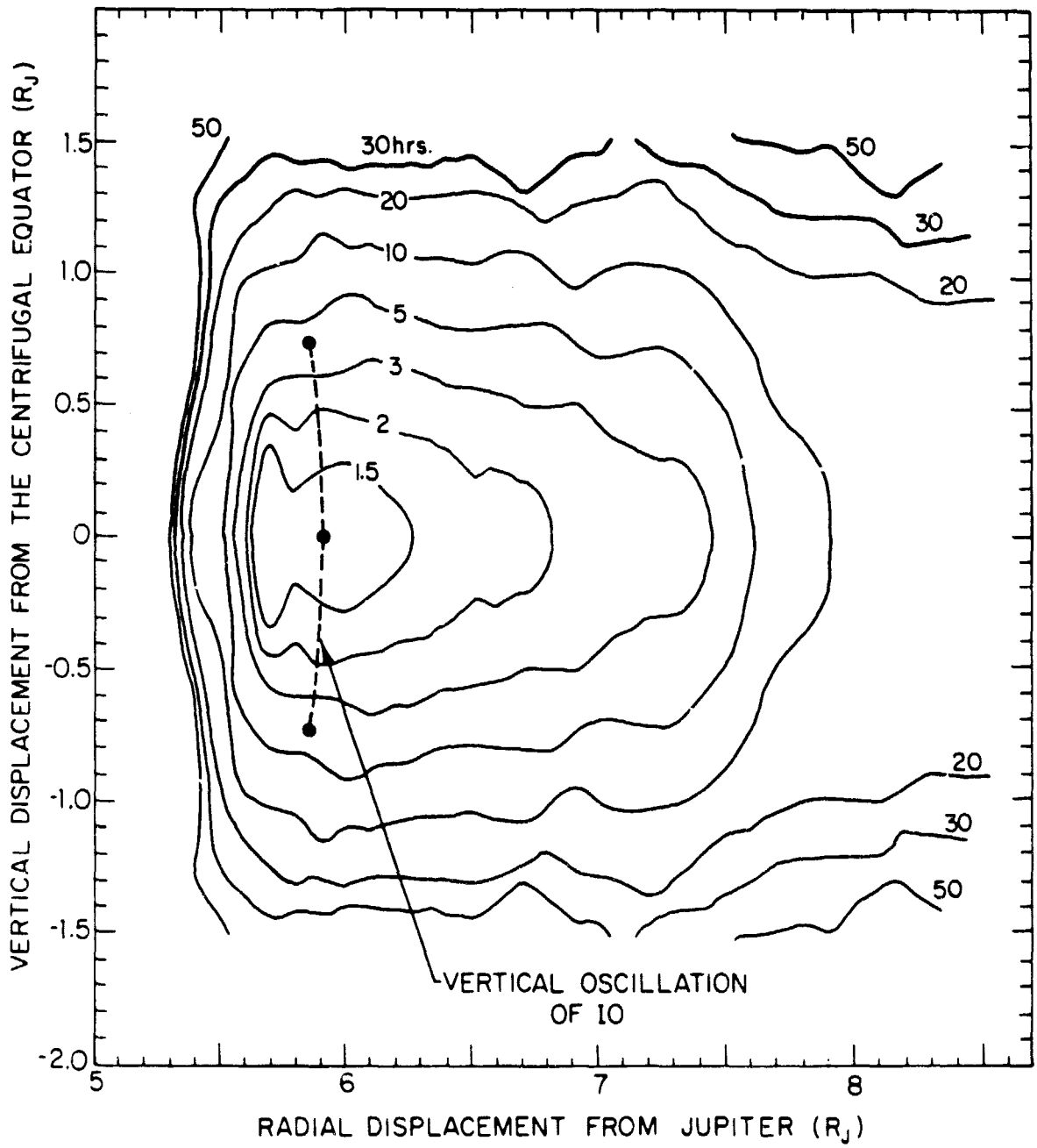

Figure 3

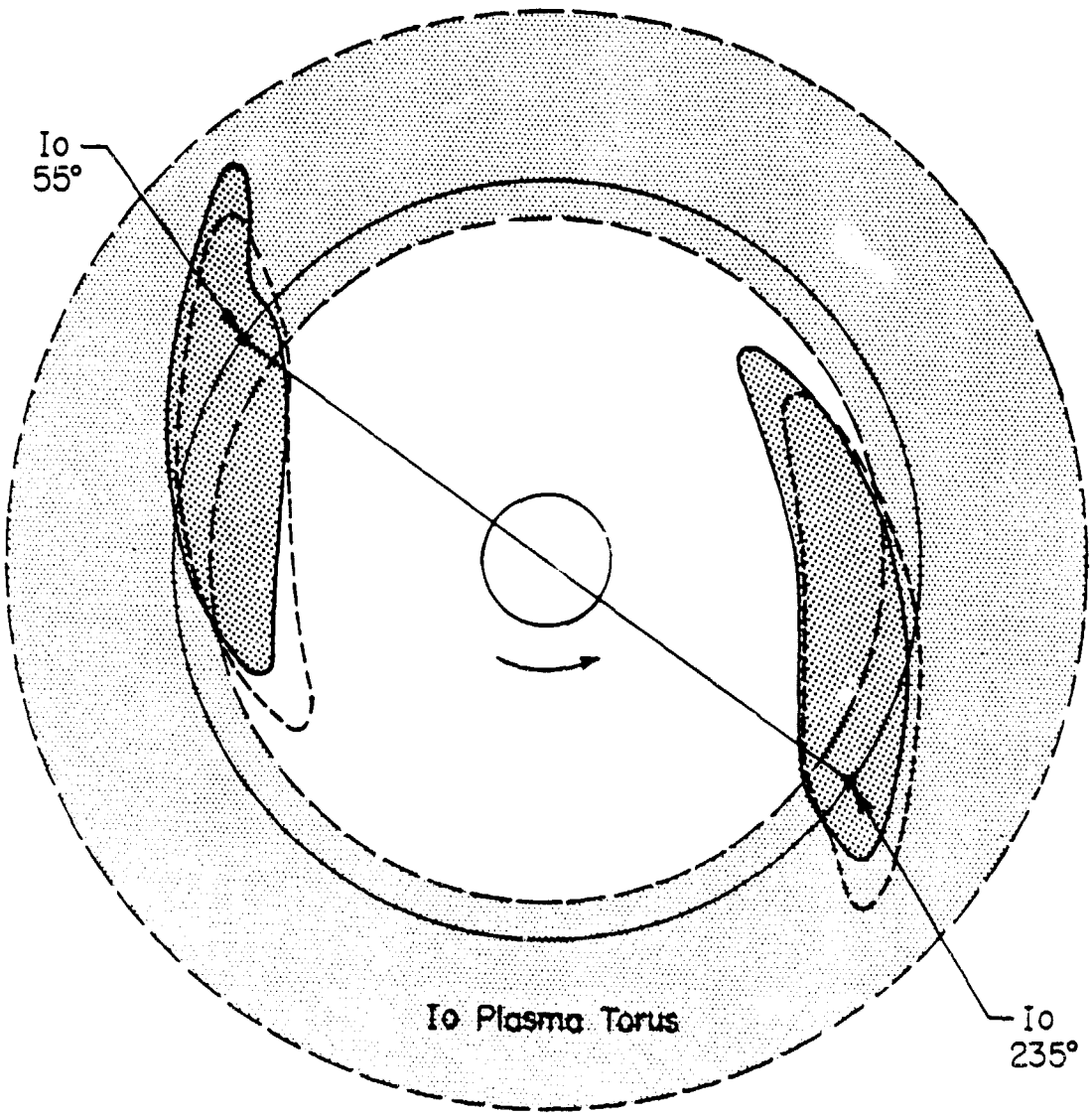

Figure 4

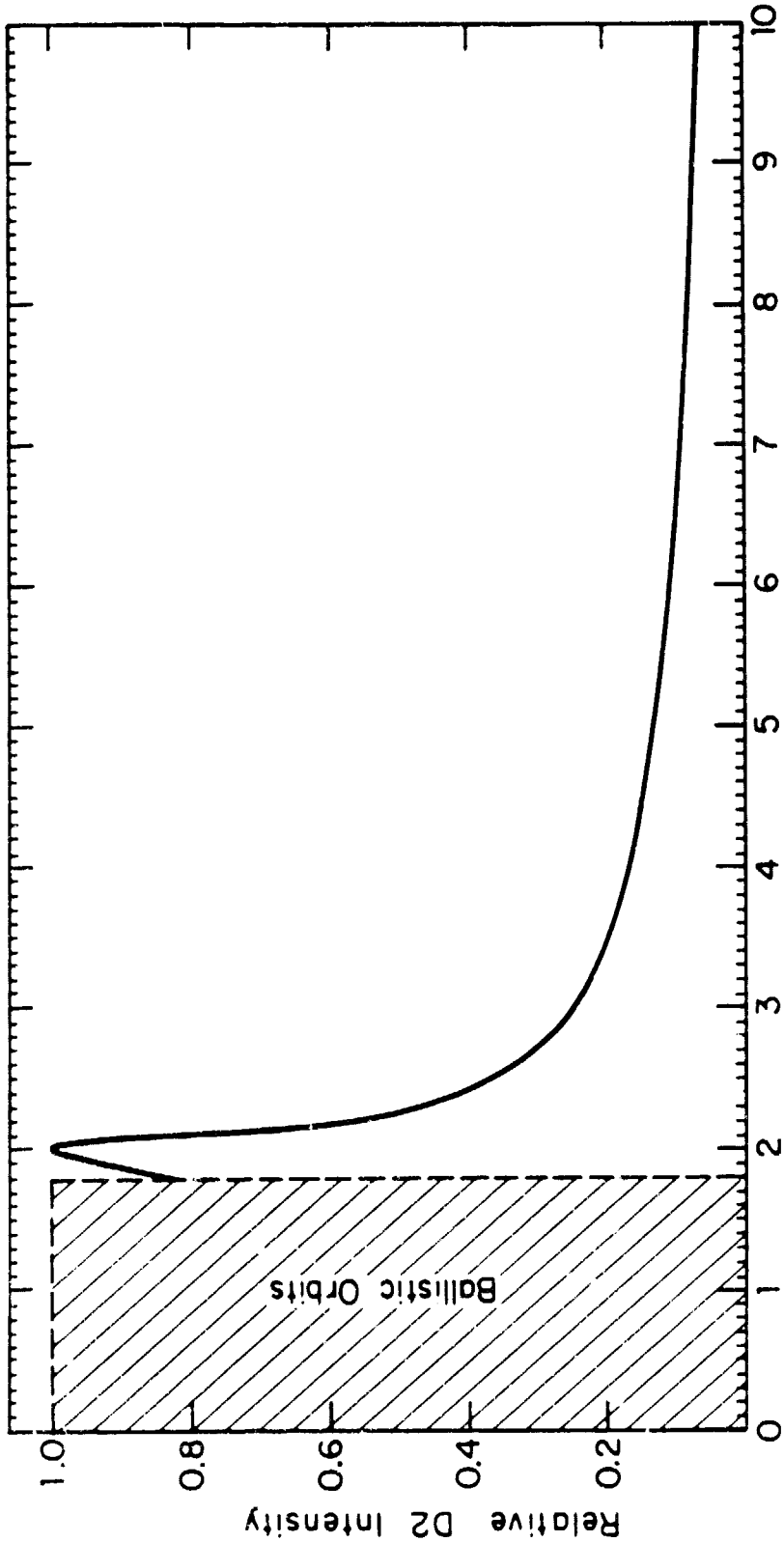

Figure 5

IO'S SODIUM CLOUD FOR A SATELLITE PHASE ANGLE OF 55°

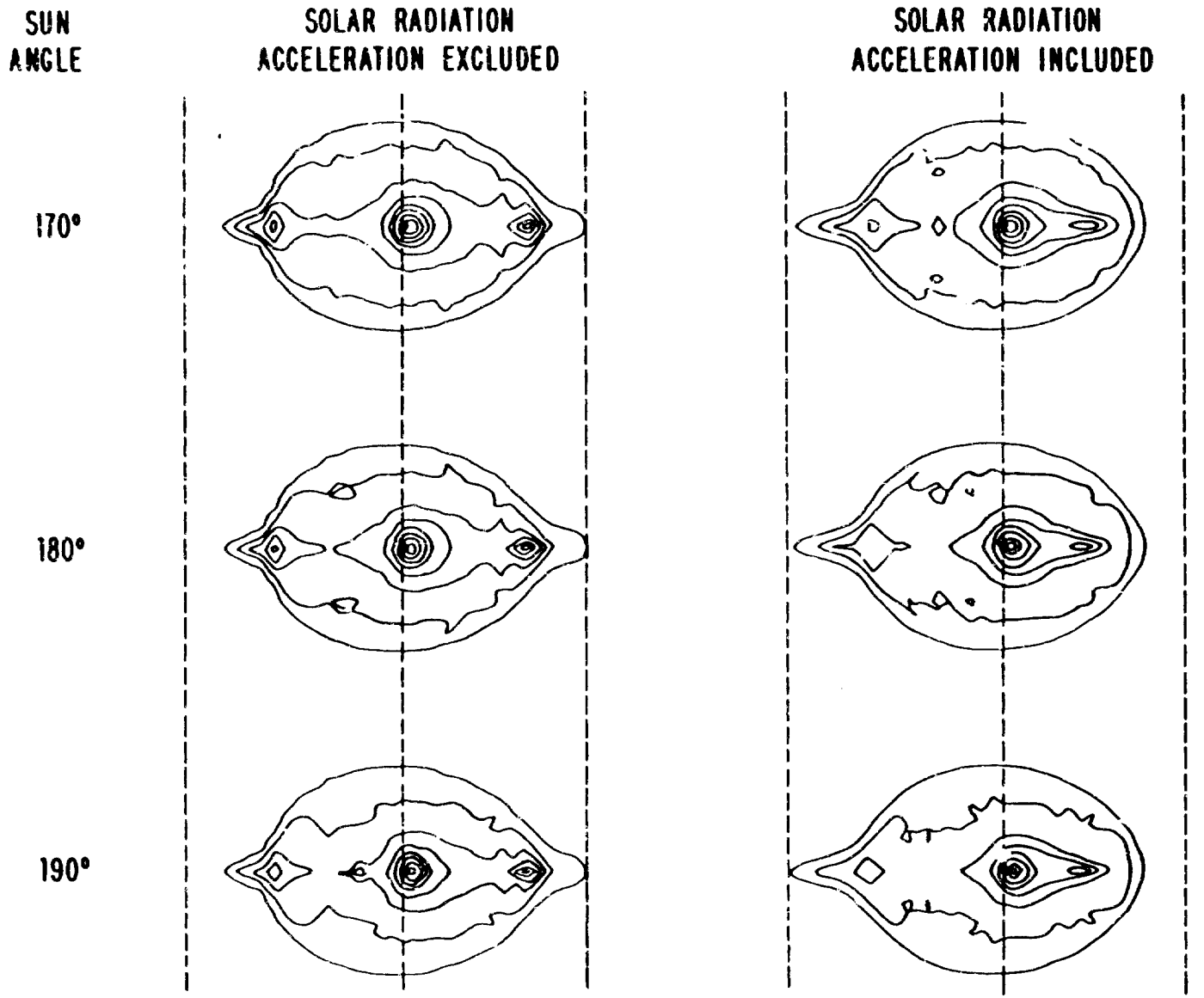

Figure 6

IO'S SODIUM CLOUD FOR A SATELLITE PHASE ANGLE OF 235°

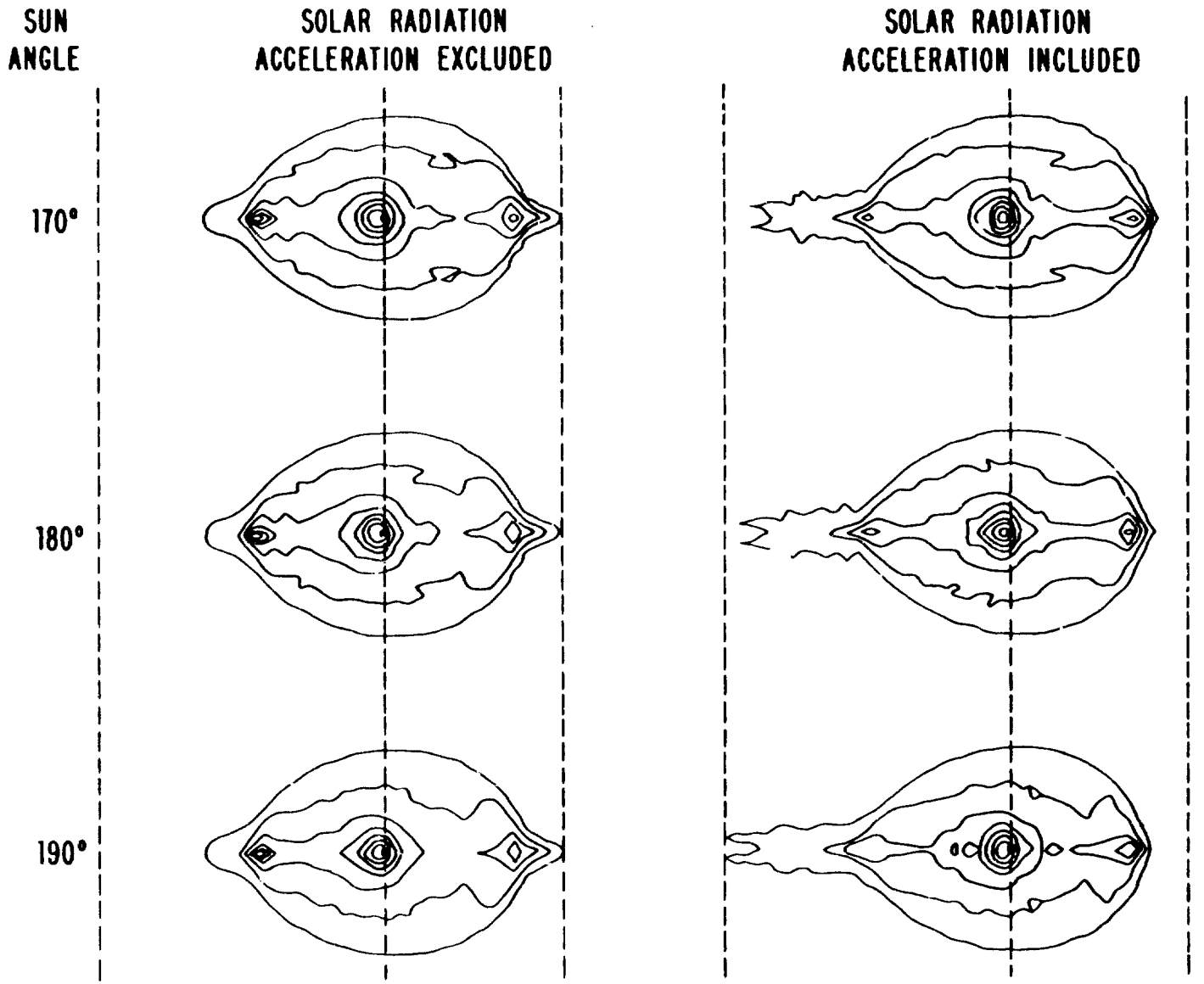

Figure 7

SODIUM CLOUD OF Io

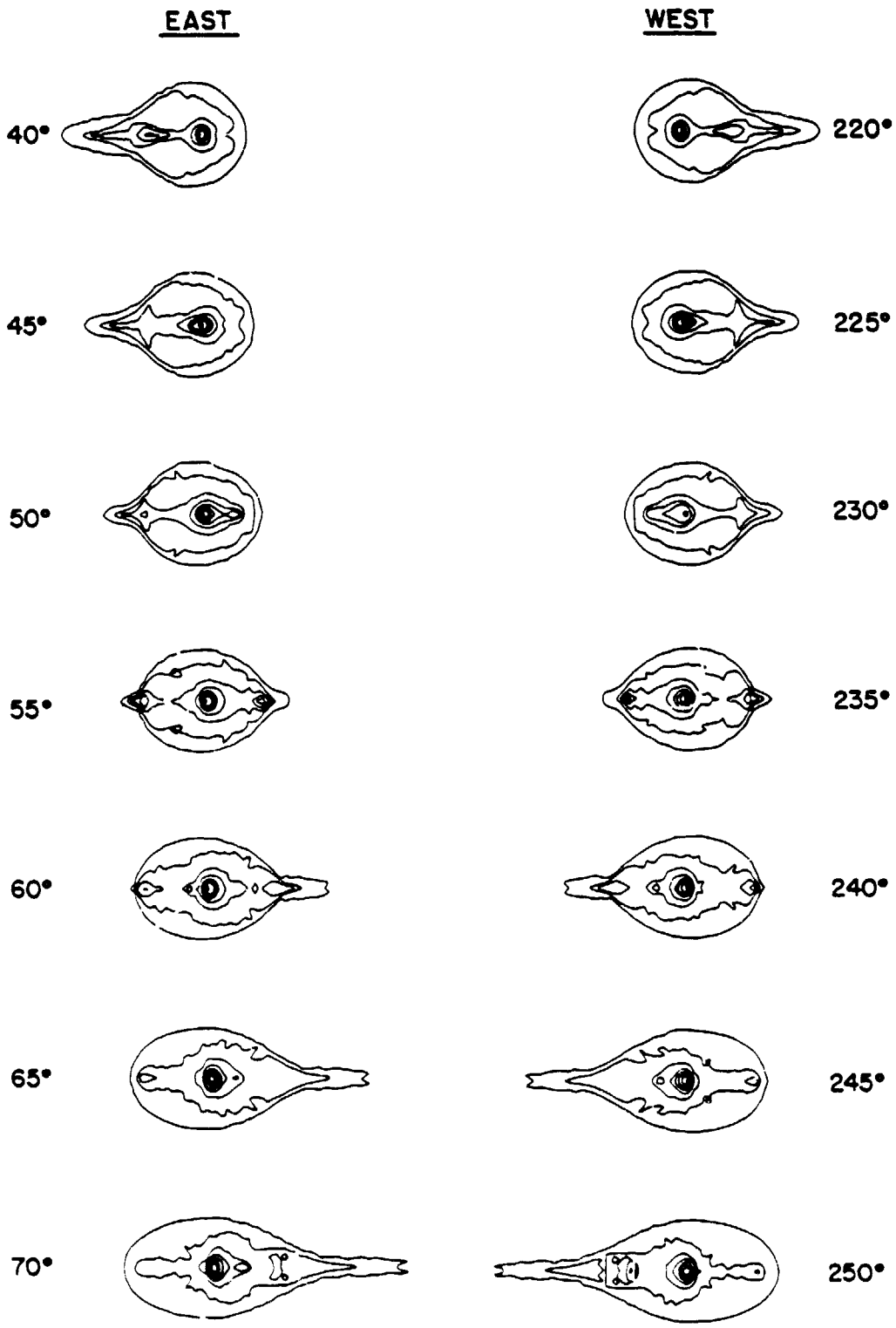

Figure 8

SODIUM CLOUD OF Io

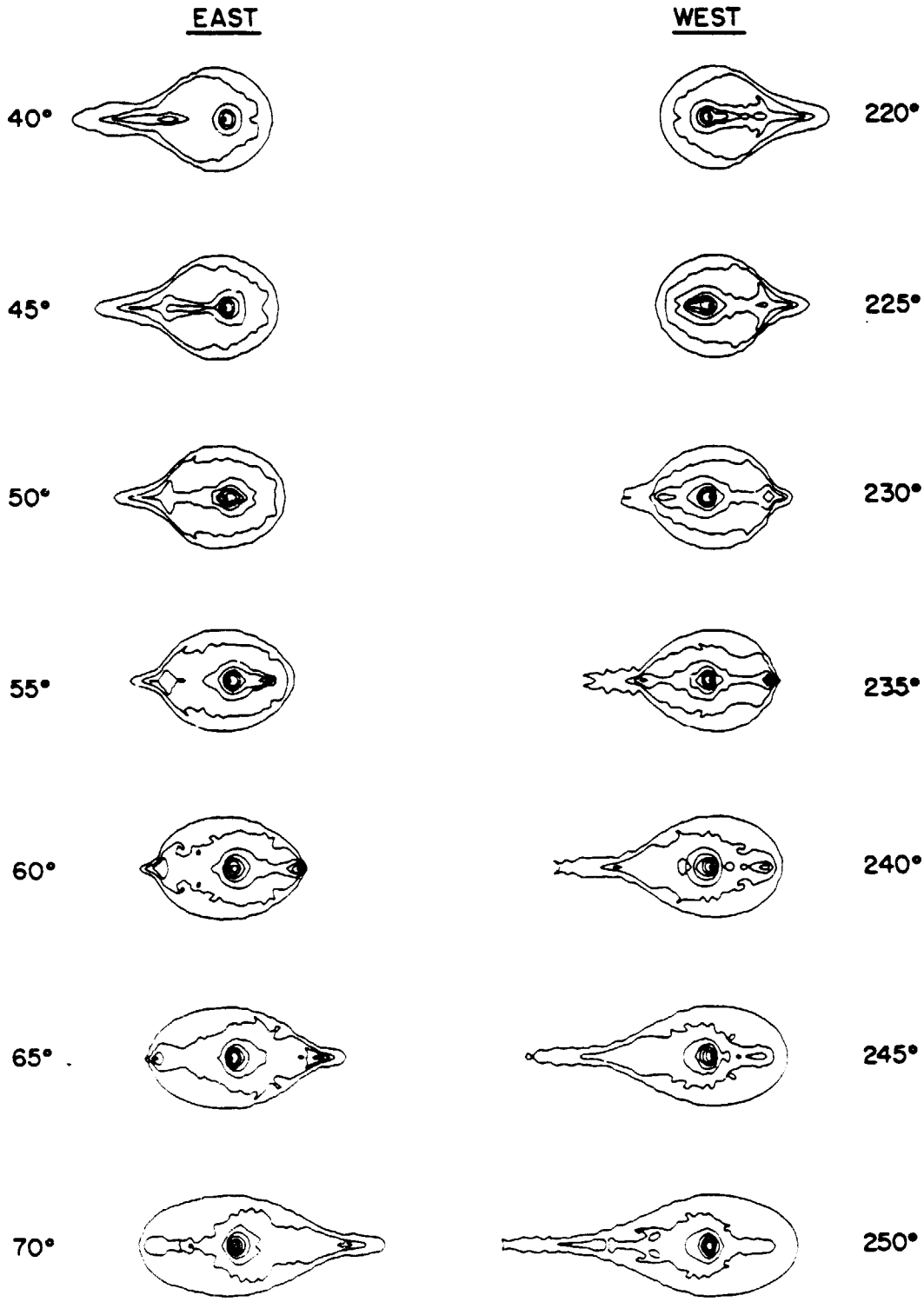

Figure 9

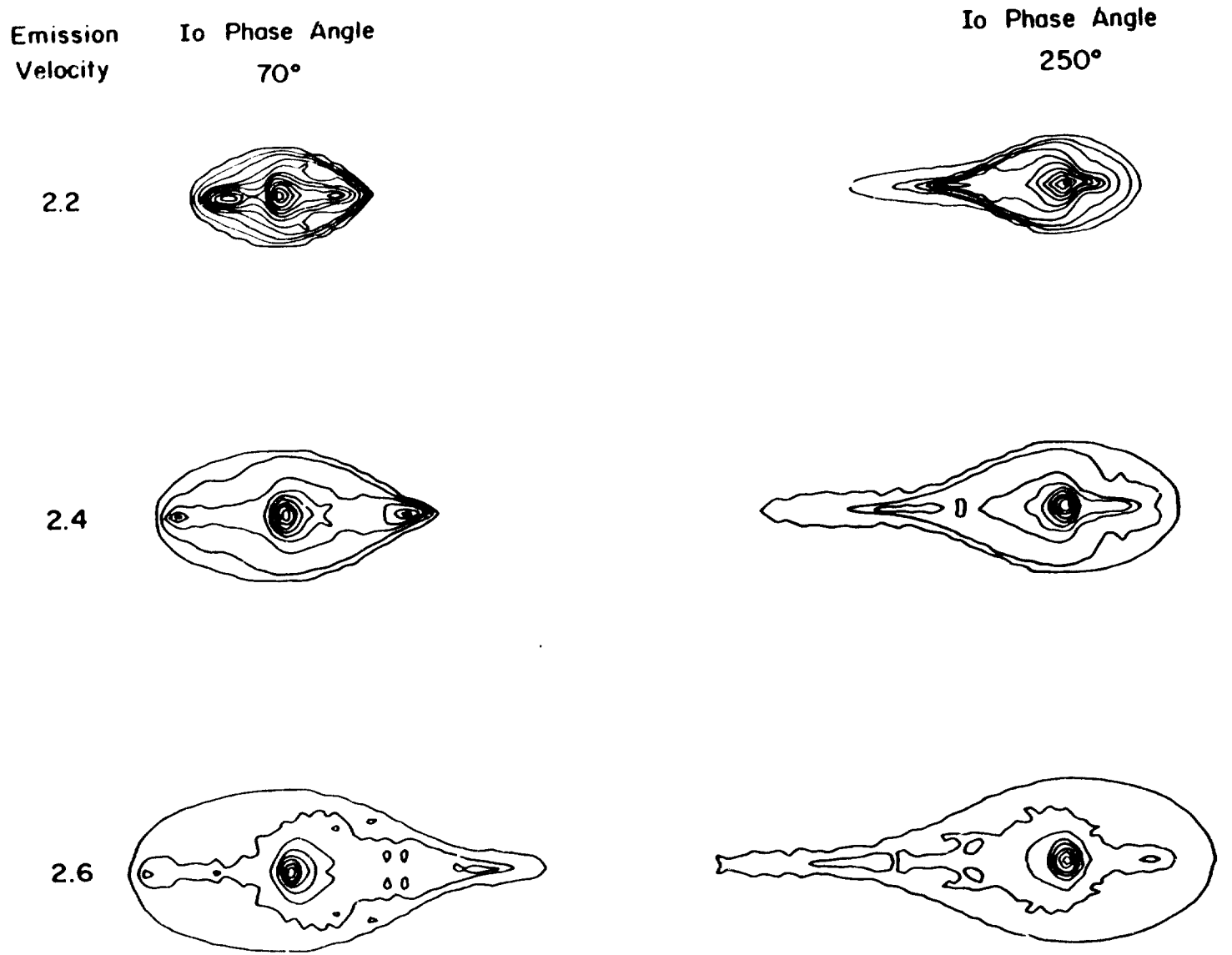

Figure 10

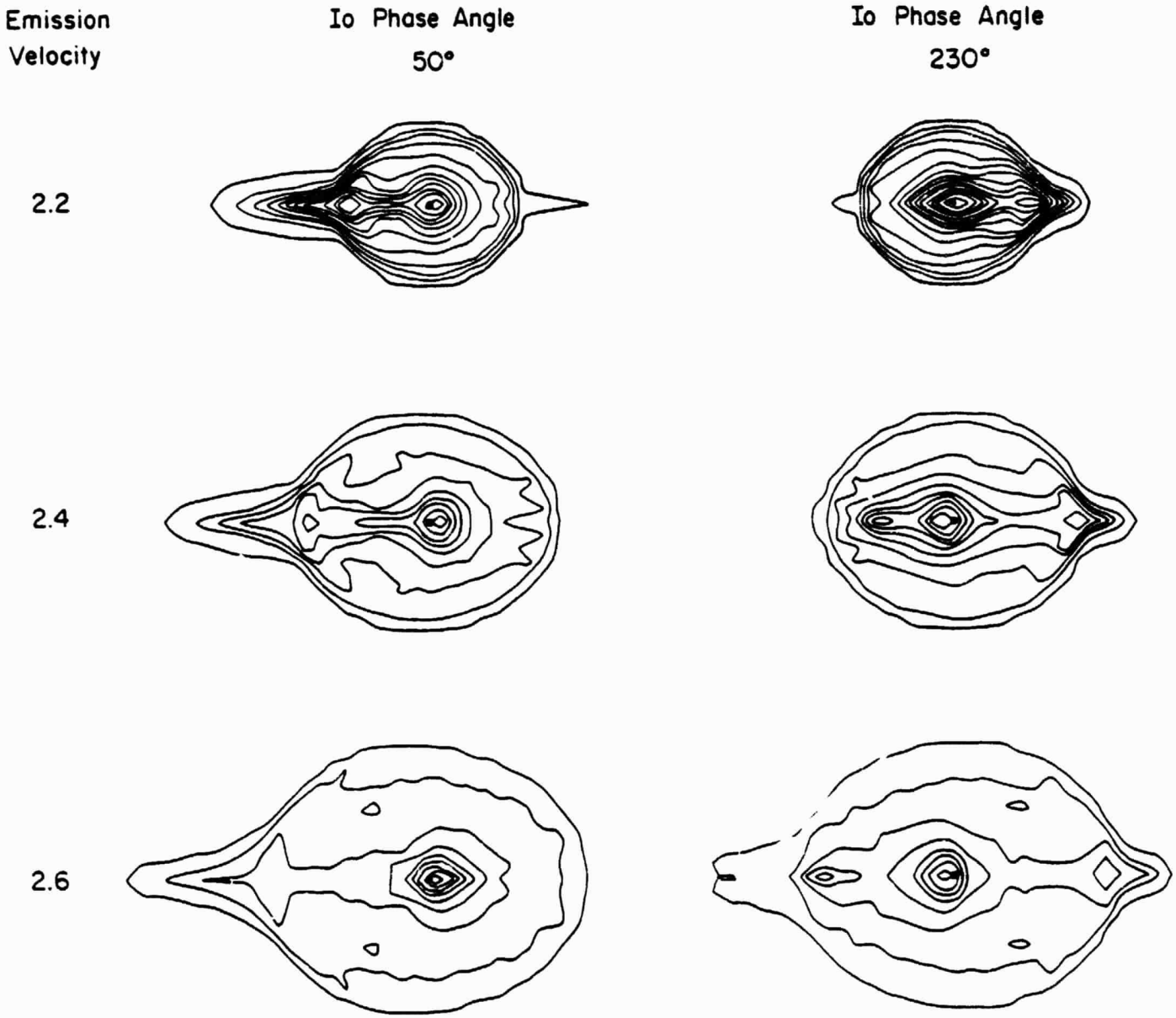

Figure 11

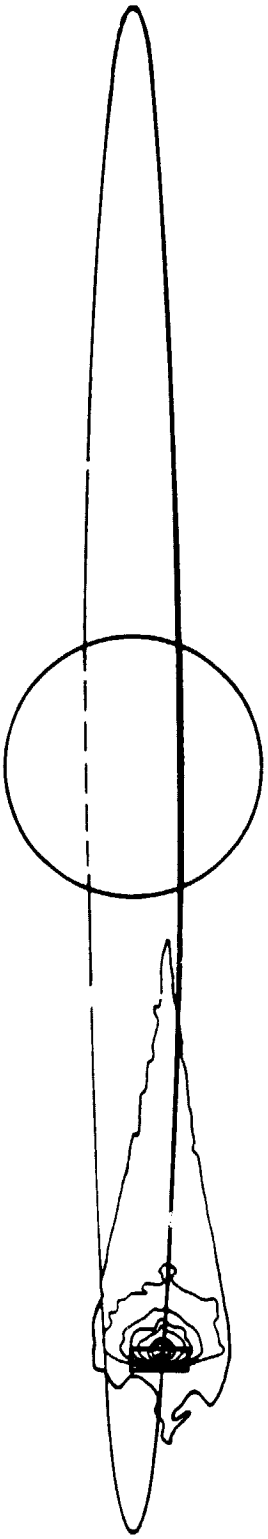

Figure 12

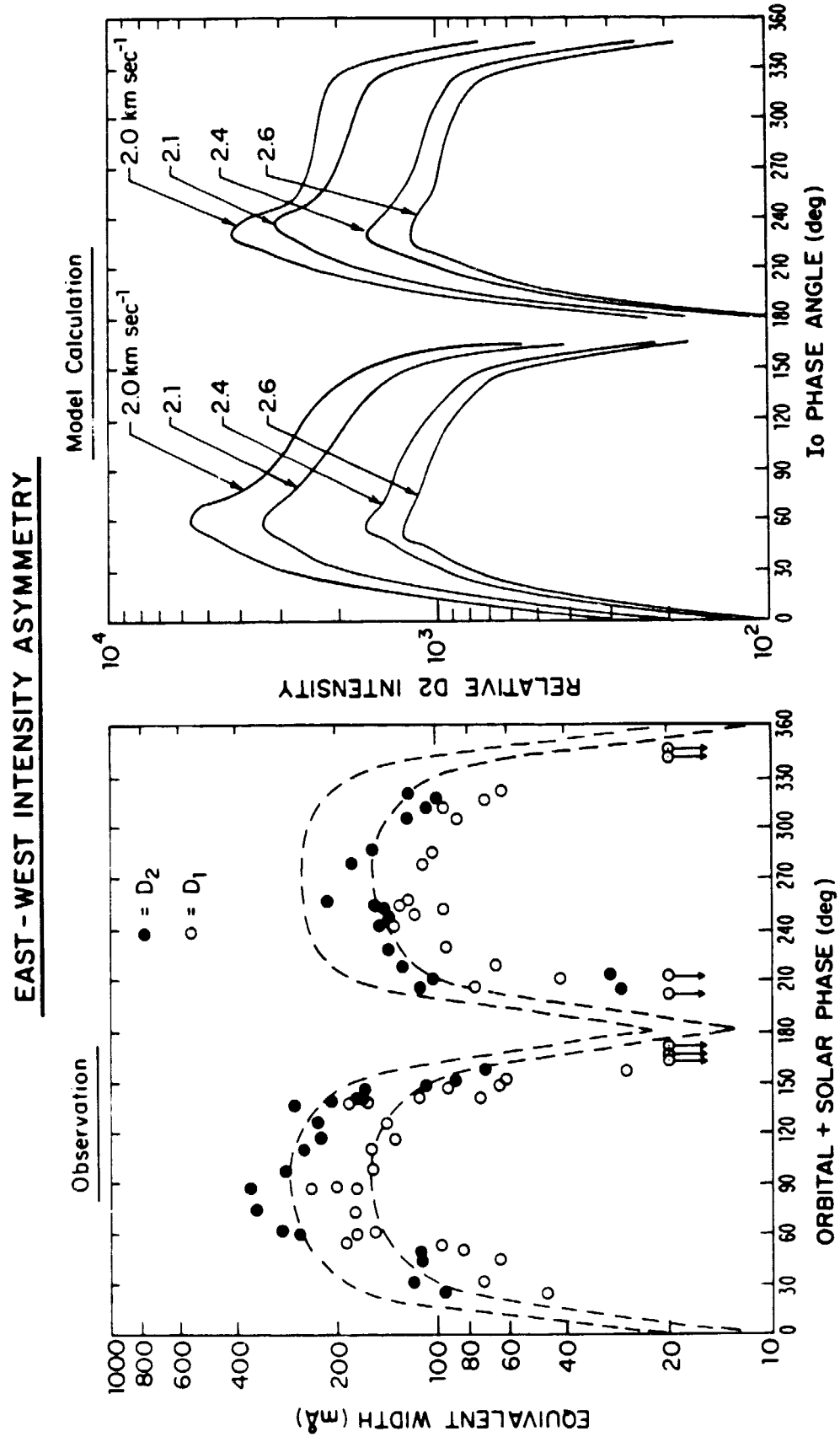

Figure 13

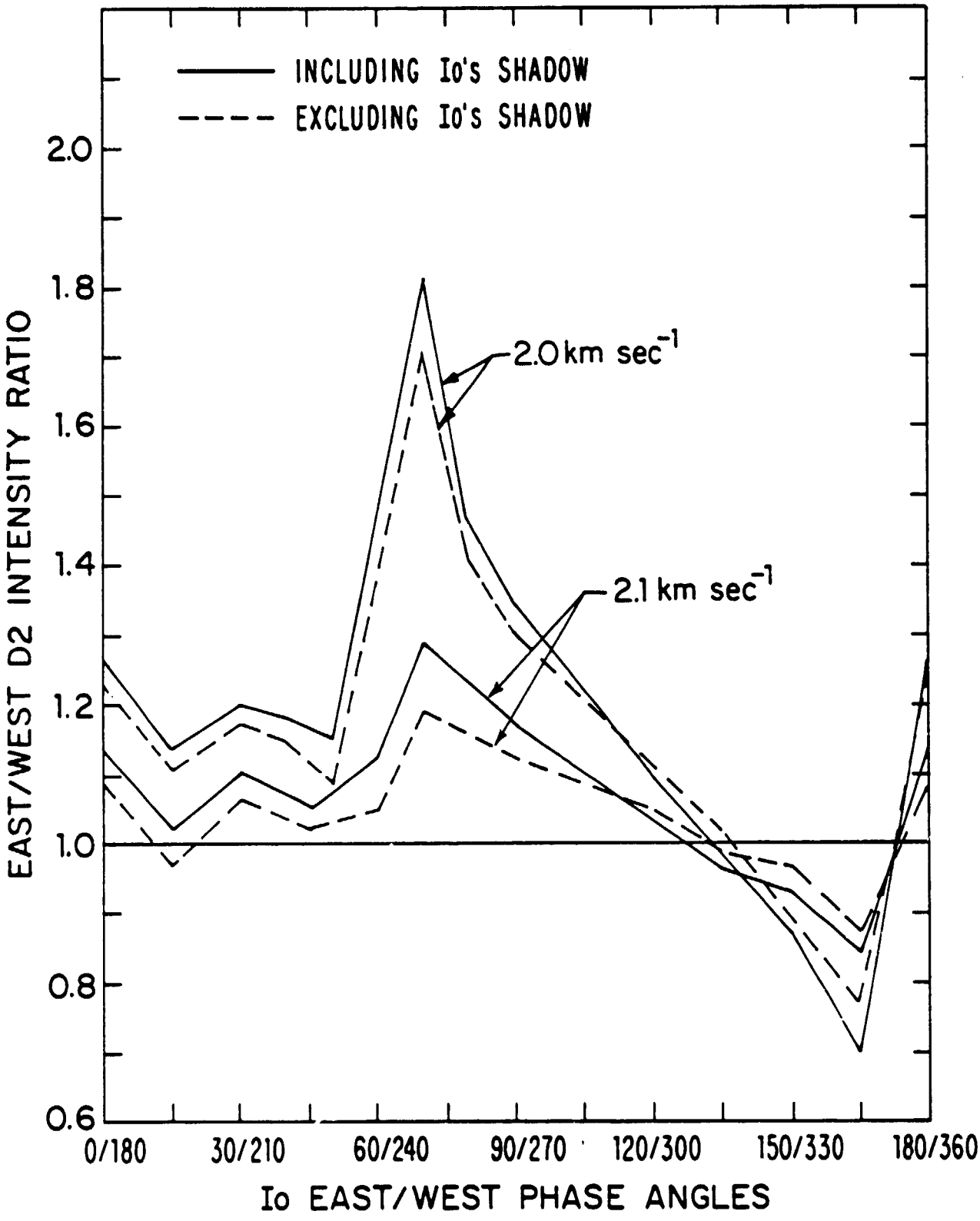

Figure 14

Figure 15

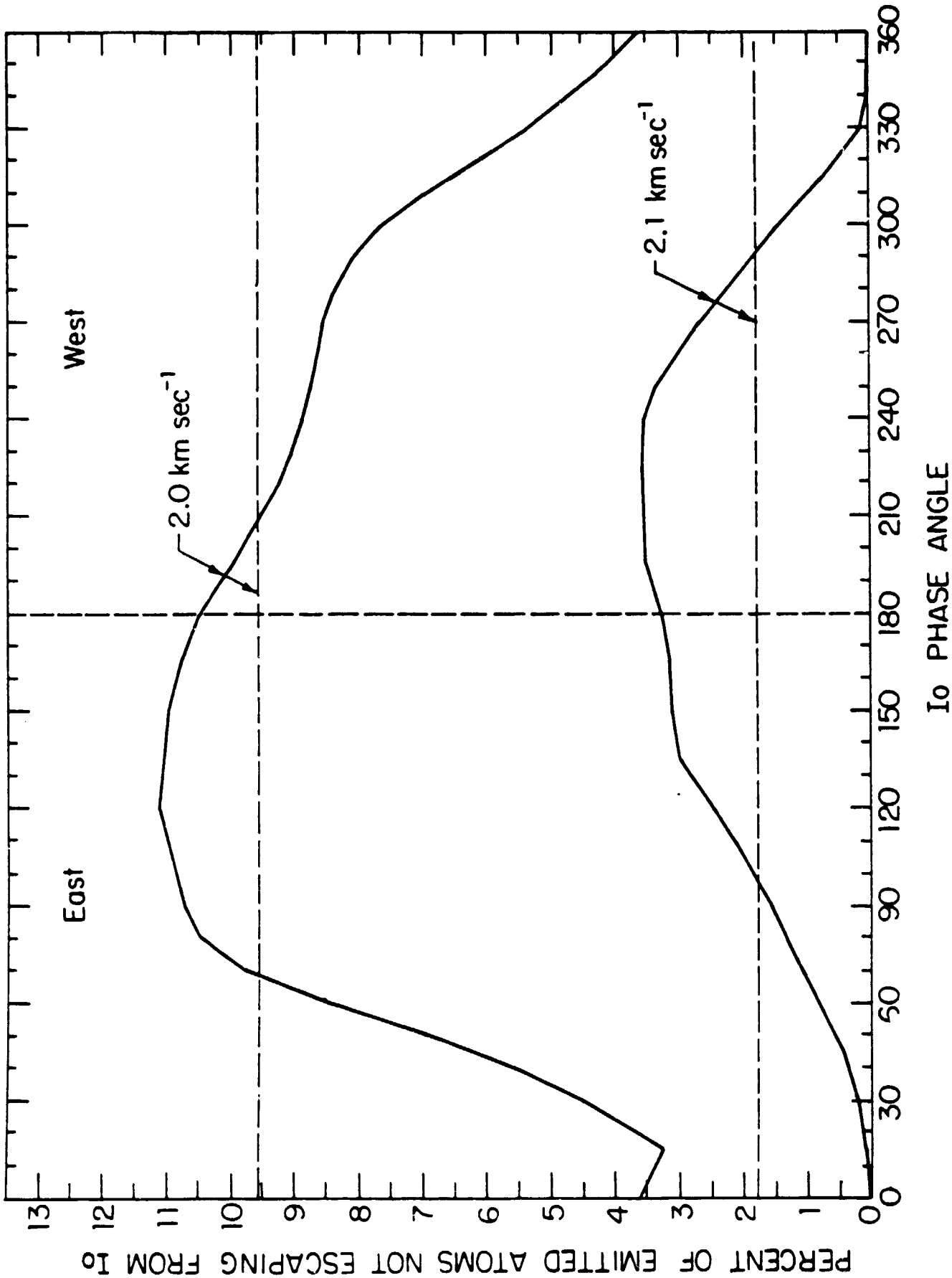

Figure 16